BRAIN FUNCTIONAL MAGNETIC RESONANCE IMAGING LATERALIZATION AND DIAGNOSTIC CLASSIFICATION IN AUTISM

by

Jared Allen Nielsen

A dissertation submitted to the faculty of
The University of Utah
in partial fulfillment of the requirements for the degree of

Doctor of Philosophy

Interdepartmental Program in Neuroscience

The University of Utah

December 2013

The University of Utah Graduate School

STATEMENT OF DISSERTATION APPROVAL

The following faculty members served as the supervisory committee chair and members for the dissertation of Jared Allen Nielsen.

Dates at right indicate the members' approval of the dissertation.

Janet E. Lainhart, Chair	July 22, 2013 Date Approved
Erin D. Bigler, Member	July 22, 2013 Date Approved
Jeffrey S. Anderson, Member	July 22, 2013 Date Approved
P. Thomas Fletcher, Member	July 22, 2013 Date Approved
Sharif Taha, Member	July 22, 2013 Date Approved

The dissertation has also been approved by Kristen Keefe Chair of the Interdepartmental Program in Neuroscience and by David B. Kieda, Dean of The Graduate School.

ABSTRACT

Systematic differences in functional connectivity magnetic resonance imaging metrics have been consistently observed in autism. I attempted to predict group membership using data provided by the Autism Brain Imaging Data Exchange, including resting state functional magnetic resonance imaging data obtained from 964 subjects and 16 separate international sites. For each of 964 subjects, I obtained pairwise functional connectivity measurements from a lattice of 7266 regions of interest covering the gray matter and attempted to classify the subjects using a leave-one-out classifier with the 26.4 million connections as features. Classification accuracy significantly outperformed chance but was much lower for multisite prediction than for previous single site results. As high as 60% accuracy was obtained for whole brain classification. Classification accuracy was significantly higher for sites with longer blood oxygen-level dependent imaging times. Attempts to use multisite classifiers will likely require improved classification algorithms, longer blood oxygen-level dependent imaging times, and standardized acquisition parameters for possible future clinical utility.

Lateralization of brain structure and function occurs in typical development and subserves functions such as language and visuospatial processing. Abnormal lateralization is present in various neuropsychiatric disorders. It has been conjectured that individuals may be left-brain dominant or right-brain dominant based on personality and cognitive style, but neuroimaging data has not provided clear evidence whether such

phenotypic differences in the strength of left-dominant or right-dominant networks exist. I evaluated whether strongly lateralized connections covaried within the same typically developing individuals (n = 1011). I also compared lateralization of functional connections in typical development and in autism. In typical development, left- and right-lateralized hubs formed two separable networks of mutually lateralized regions. Connections involving only left- or only right-lateralized hubs showed positive correlation across subjects, but only for connections sharing a node. Our data are not consistent with a whole-brain phenotype of greater "left-brained" or greater "right-brained" network strength across individuals. The autism group lacked left lateralization in three connections involving language regions and regions from the default mode network. Abnormal language lateralization in autism may be due to abnormal language development rather than a deficit in hemispheric specialization of the entire brain.

TABLE OF CONTENTS

LIST OF TABLES

LIST OF FIGURES

ACKNOWLEDGMENTS

I have many people I would like to thank and acknowledge. Without their help none of these studies would have been possible. I would like to thank my dissertation committee, especially Janet Lainhart and Jeff Anderson; the Interdepartmental Program in Neuroscience, especially Kristen Keefe, Mary Lucero, and Tracy Marble; the other graduate students and staff in the lab; and most of all my family, especially my wife, Kiersten. The analyses described were supported by NIH grant numbers T32DC008553, R01MH084795, and R01MH080826. Finally, I would like to sincerely thank the children, adolescents, and adults with autism, the individuals with typical development, and all the families who participated in these studies.

CHAPTER 1

INTRODUCTION

With a better understanding of the underlying neural differences in individuals with autism, a faster, more objective, biologically-based diagnostic test could be implemented. Currently, diagnosis is made with only a clinical observation session of the patient and an interview of someone close to the patient (Lord et al., 2000; Lord, Rutter, & Le Couteur, 1994). The diagnosis requires multiple hours of careful analysis. Diagnostic accuracy depends upon clinician training, interviewer training, and interviewee reliability.

Observations of abnormal neural synchrony in autism have become more and more common in scientific literature. In task-related functional connectivity studies, individuals with autism had decreased connectivity in the motor execution network during a motor task (Mostofsky et al., 2009a), in the cortical language system during a sentence comprehension task (Just, Cherkassky, Keller, & Minshew, 2004), in connections between the fusiform face area and other limbic structures during a face identification task (Kleinhans et al., 2008), and in connections between the parietal lobe and other brain regions during a working memory task (Koshino et al., 2005). In resting state functional connectivity studies, the autism group was marked by decreased connectivity in the default mode network (Assaf et al., 2010; Kennedy & Courchesne,

2008a, 2008b; Kennedy, Redcay, & Courchesne, 2006; Monk et al., 2009; Weng et al., 2010). The default mode network is a set of brain regions that consistently increase in activity at rest and decrease in activity during cognitive tasks performed in the scanner. Along with the default mode network, our lab has found differences in interhemispheric connections of homologous brain regions (Anderson et al., 2011). Understanding where differences in functional connectivity exist and when the differences occur will help single out which brain networks to target for pharmacological studies and when the treatments would be most needed and/or effective.

In addition to reports of abnormal neural synchrony, there are ample reports of abnormal lateralization of brain structure and function in autism (Anderson et al., 2010; Lange et al., 2010b). The initial reports on lateralization of brain function conducted by Paul Broca and Karl Wernicke found that language function in their patients was localized to the left hemisphere. More recent studies report that ~95% of right-handed and ~75% of left-handed individuals have language function localized to the left hemisphere, and handedness relates significantly to lateralization of language function (Knecht et al., 2000a; Knecht et al., 2000b). Because of the strong link between brain lateralization and language and between autism and language, the overwhelming majority of studies investigating autism and abnormal lateralization have restricted their analyses to core brain regions involved in language processing.

The purpose of this dissertation is three-fold:

1) Develop a multisite diagnostic classifier using functional connectivity MRI.
2) Identify lateralized brain networks in healthy controls and compare the synchrony

of these networks to those of individuals with autism.

3) Determine whether “left-brain” and “right-brain” phenotypes exist.

CHAPTER 2

MULTISITE FUNCTIONAL CONNECTIVITY MRI CLASSIFICATION OF AUTISM: ABIDE RESULTS

Brain imaging classification strategies of autism have used information from structural MRI (Calderoni et al., 2012; Ecker et al., 2010a; Ecker et al., 2010b; Jiao et al., 2010; Sato et al., 2013; Uddin et al., 2011), functional MRI (Anderson et al., 2011d; Coutanche, Thompson-Schill, & Schultz, 2011; Wang, Chen, & Fushing, 2012), diffusion tensor MRI (Ingalhalikar, Parker, Bloy, Roberts, & Verma, 2011; Lange et al., 2010a), positron emission tomography (Duchesnay et al., 2011), and magnetoencephalography (Khan et al., 2013; Roberts et al., 2011; Roberts et al., 2010; Tsiaras et al., 2011). Such approaches have been undertaken for several clinical objectives. Sensitive and specific biomarkers for autism may contribute potentially useful biological information to diagnosis, prognosis, and treatment decision-making. It is hoped that imaging biomarkers may also help delineate subtypes of individuals with autism that may have common brain neuropathology and respond to similar treatment strategies, although different methodology will likely be required for subgrouping individuals than for classifying individuals by diagnosis. Such quantitative biomarkers may also serve as a metric for biological efficacy of potential behavioral or pharmacologic interventions. Finally,

imaging biomarkers may help identify pathophysiologic mechanisms of autism in the brain that can guide investigations into the specific neural circuits, developmental windows, and genetic or environmental factors that may result in improved treatments.

Abnormal functional connectivity MRI (fcMRI) has been among the most replicated imaging metrics in autism. The proposed basis for fcMRI is that connected brain regions are likely to exhibit synchronized neural activity, which can be detected as covariance of slow fluctuations in blood oxygen level dependent (BOLD) signal between the regions. Initial reports of decreased functional connectivity in autism by three independent groups (Just et al., 2004; Villalobos, Mizuno, Dahl, Kemmotsu, & Muller, 2005; Welchew et al., 2005) have been followed by more than 50 primary reports of abnormal functional connectivity in autism in the literature, derived from fMRI data both in a resting state and acquired during cognitive tasks (Anderson, 2013).

Most reports show decreases in connectivity between distant brain regions, including nodes of the brain's default mode network (Cherkassky, Kana, Keller, & Just, 2006; Kennedy & Courchesne, 2008b; Wiggins et al., 2011), social brain regions (Gotts et al., 2012; von dem Hagen, Stoyanova, Baron-Cohen, & Calder, 2012), attentional regions (Koshino et al., 2005), language regions (Dinstein et al., 2011), interhemispheric homologues (Anderson et al., 2011), and throughout the brain (Anderson et al., 2011d). Nevertheless, some reports have also shown abnormal increases in functional connectivity in autism (Muller et al., 2011) or unchanged connectivity (Tyszka, Kennedy, Paul, & Adolphs, 2013). In particular, higher correlation between brain regions has been observed in negatively correlated connections (Anderson et al., 2011d), corticostriatal connections (Di Martino et al., 2011), visual search regions (Keehn, Shih, Brenner,

Townsend, & Muller, 2012), and brain network-level metrics (Anderson, Ferguson, & Nielsen, 2013a; Lynch et al., 2013).

Despite the large and growing body of reports of abnormal functional connectivity in autism, uncertainty remains about the spatial distribution of decreased and increased connectivity and how this relates to the clinical heterogeneity of autism spectrum disorders (ASD). One of the challenges for answering these questions has been fractionation of the available data into individual site-specific studies with relatively small sample sizes. There is a need for analysis of multisite datasets that can improve statistical power, represent greater variance of disease and control samples, and allow replication across multiple sites with differential subject recruitment, imaging parameters, and analysis methods. Ultimately, clinically useful biomarkers will need to be replicated in diverse acquisition conditions that reflect community and academic imaging practices.

The advent of cooperative, publicly available datasets for resting state functional MRI is an important step forward. Multiple such datasets have now been released including the 1000 functional connectome project (Biswal et al., 2010), the attention deficit 200 Consortium dataset (ADHD-200_Consortium, 2012), and most recently the Autism Brain Imaging Data Exchange (ABIDE; (Di Martino et al., 2013), consisting of images from 539 individuals with ASD and 573 typical control individuals, acquired at 16 international sites. In the present study, we evaluate classification accuracy of whole-brain functional connectivity across sites, and determine which abnormalities in connectivity across the brain are most informative for predicting autism from typical development, which imaging acquisition features lead to greatest accuracy, whether

functional connectivity abnormalities covary with metrics of disease severity, and the extent to which abnormal functional connectivity is replicated across sites.

Materials and Methods

Subject Sample

ABIDE consists of 1112 datasets comprised of 539 autism and 573 typically developing individuals (Di Martino et al., 2013). Each dataset consists of one or more resting fMRI acquisitions and a volumetric MPRAGE image. All data are fully anonymized in accordance with HIPAA guidelines, with analyses performed in accordance with pre-approved procedures by the University of Utah Institutional Review Board. All images were obtained with informed consent according to procedures established by human subjects research boards at each participating institution. Details of acquisition, informed consent, and site-specific protocols are available at http://fcon_1000.projects.nitrc.org/indi/abide/.

Inclusion criteria for subjects were successful preprocessing with manual visual inspection of normalization to Montreal Neurologic Institute (MNI) space of the magnetization prepared rapid gradient echo (MPRAGE) image, coregistration of BOLD and MPRAGE images, segmentation of MPRAGE image, and full brain coverage from MNI $z>-35$ to $z<70$ on all BOLD images. Inclusion criteria for sites were a total of at least 20 subjects meeting all other inclusion criteria. A total of 964 subjects met all inclusion criteria (517 typically developing subjects and 447 subjects with autism from 16 sites). Each site followed different criteria for diagnosing patients with autism or ascertaining typical development, however, the majority of the sites used the Autism

Diagnostic Observation Schedule (Lord et al., 2000) and Autism Diagnostic Interview-Revised (Lord et al., 1994). Specific diagnostic criteria for each site can be found at fcon_1000.projects.nitrc.org/indi/abide/index.html.

Subject demographics for individuals satisfying inclusion criteria are shown in Table 2.1. Six different testing batteries were used to calculate verbal IQ and performance IQ, respectively. In addition to the IQ measures, the following measures were included in correlations with the classifier score (see Table 2.1 for summary of behavioral measures): the Social Responsiveness Scale (Constantino & Todd, 2003) is a measure of social function and the Vineland Adaptive Behavior Scales (Sparrow, Balla, & Cicchetti, 1984) is a measure of daily functioning. See the ABIDE website for more information on the specific behavioral measures used. For handedness, categorical handedness (i.e, right-handed, left-handed, or ambidextrous) was used in the leave-one-out classifier (see details below). In the case that only a quantitative handedness measure was reported, positive values were converted to right-handed, negative values to left-handed, and a value of zero to ambidextrous. Fifteen subjects lacked a categorical and quantitative measure of handedness. In those cases, a nearest neighbor classification function (ClassificationKNN.m in MATLAB) was used to assign categorical handedness. For the classifier, 862 subjects were right-handed, 95 were left-handed, and 7 were ambidextrous.

BOLD Preprocessing

Preprocessing was performed in MATLAB (Mathworks, Natick, MA) using SPM8 (Wellcome Trust, London) software. The following sequence of preprocessing steps was performed:

1) Slice timing correction
2) Realign and reslice correction of motion for each volume relative to initial volume
3) Coregistration of BOLD images to MPRAGE anatomic sequence
4) Normalization of MPRAGE to MNI template brain, with normalization transformation also applied to coregistered BOLD images
5) Segmentation of gray matter, white matter, and cerebral spinal fluid (CSF) components of MPRAGE image (thorough clean)
6) Voxelwise bandpass filter (0.001 to 0.1 Hz) and linear detrend
    a. The lower limit of 0.001 Hz was chosen in order to be certain as much neural information was included as possible (Anderson, Zielinski, Nielsen, & Ferguson, 2013c). The linear detrend removed much of the contribution of low frequencies given the relatively short time series available in the dataset.
7) Extraction of mean time courses from the restriction masks applied to BOLD images from ROIs consisting of:
    a. CSF segmented mask with bounding box $-35<x<35$, $-60<y<30$, $0<z<30$
    b. White matter segmented mask overlapping with 10 mm radii spheres centered at x=-27,y=-7,z=30, x=27, y=-7,z=30
    c. Mask of scalp and facial soft tissues (Anderson et al., 2011a)

8) Voxelwise regression using glmfit.m (MATLAB Statistics Toolbox) software of CSF, WM, Soft tissue, and 6 motion parameters from realignment step from time series of each voxel of BOLD images
9) Motion scrubbing (Power, Barnes, Snyder, Schlaggar, & Petersen, 2012) of framewise displacement and DVARS with removal of volumes before and after a root-mean-square displacement of >0.2 mm for either parameter and concatenation of remaining volumes. In 86.2% of the participants more than 50% of the volumes remained after motion scrubbing. Among the remaining participants with fewer than 50% retained volumes, the majority belonged to the autism group (8.8%, compared to 5.0% from the typically developing group; p = 0.02). The groups differed in the number of retained volumes when considering the entire sample of 964 subjects ($t = 4.11$, $p < 0.001$) and when considering only those with greater than 50% of the volumes remaining ($t = 2.04$, $p = 0.04$).
10) No spatial smoothing was performed. The global mean signal and gray matter time courses were not regressed from voxelwise data (Jo, Saad, Gotts, Martin, & Cox, 2013; Saad et al., 2013; Saad et al., 2012).

ROI Analysis

From preprocessed BOLD images for each subject, mean time course was extracted from 7266 gray matter regions of interest (ROIs). These ROIs from a lattice covering the grey.nii image (SPM8) from z=-35 to z= 70 at 5-mm resolution, with MNI coordinates of centroids previously reported (Anderson et al., 2011d). The ROIs averaged 4.9 +/- 1.3 standard deviation voxels in size for 3 mm isotropic voxels. A 7266 x 7266

matrix of Fisher-transformed Pearson correlation coefficients was obtained for each subject from the ROI timecourses representing an association matrix of functional connectivity in each subject between all pairs of ROIs. Each pair of ROIs is termed a "connection" for the present analysis.

Leave-One-Out Classifier

The classification approach is summarized in Figure 2.1. Overall, a leave-one-out classifier was used to generate a classification score for each of the 964 subjects, leaving out one subject at a time and calculating the classification score for the left out subject. The classification approach followed the approach reported previously, with slight modifications (Anderson et al., 2011d). First, the correlation measurements for the remaining 963 subjects were extracted for one of the 26.4 million connections from the 7266 x 7266 association matrix described above (Figure 2.1, Step 1). Second, a general linear model was fit to the measurements separately for autism (red fit line in Figure 2.1, Step 2) and control subjects (black fit line in Figure 2.1, Step 2) for the given connection with covariates of subject age, age-squared, gender, and handedness. From these data, estimated values for the left out subject for this connection were calculated based on the left out subject's age, gender, and handedness. A value was estimated separately from the remaining autism subjects (blue X in Figure 2.1, Step 2) and remaining control subjects (green X in Figure 2.1, Step 2).

Because each site used slightly different scanning hardware and parameters that may systematically bias results, the estimated values of the left out subject (blue and green X in Figure 2.1, Step 2) were adjusted by adding the difference of the site's mean

value for that connection (minus the left out subject) from the mean value for that connection from all other sites. Finally, the actual value for the left out subject for the connection (green dot in Figure 2.1, Step 2) was subtracted from the estimated value obtained from autism subjects (blue vertical line on Figure 2.1, Step 2) and from the estimated value obtained from control subjects (green vertical line in Figure 2.1, Step 2). The difference of the absolute value of these two differences was then multiplied by the F-statistic for the difference between the remaining autism and control subjects. This process was iteratively carried out for all 26.4 million connections and then averaged across the 7265 connections in which each of 7266 ROIs participates. Then the averaged values for each of the 7266 ROIs were summed. The summed value was equal to the classification score for the subject. More negative values for the classification score predict the left out subject was a control subject, and more positive values for classification score predict the left-out subject was an autism subject.

Bins of "Connections"

Connections were grouped into bins in several different ways to aggregate groups of connections to test for accuracy in discriminating autism from control subjects. First, a measurement of correlation strength was obtained for each connection from 961 independent subjects from the 1000 Functional Connectome project using identical preprocessing steps. Subjects included in this sample have been previously described (Ferguson & Anderson, 2011). Second, Euclidean distance between each pair of ROIs was calculated from the centroid coordinates for the ROIs. Connections were grouped into two-dimensional bins based on the strength of the correlation and the distance

between the ROIs, with bin spacing of 0.05 units of Fisher-transformed correlation and 5-mm distance.

A separate binning scheme was performed during the evaluation of a leave-one-out-classifier. For each left out subject, sets of connections were calculated that satisfied a two-tailed *t*-test between remaining autism and control subjects with *p*-values less than 0.01, 0.001, 0.0001, and 0.00001. These sets of connections varied slightly for each left out subject, since no data that can reflect the value of the left-out subject's connectivity measurement can be used in the classifier.

Classification accuracy, sensitivity, and specificity were calculated for the set of connections that differed between autism and control subjects at *p*-values of 0.01, 0.001, 0.0001, 0.00001. We used this last binning system because there is a tradeoff in using many connections in constructing the classifier scores and using fewer but more informative connections. We wanted to determine which thresholded bin yielded the highest accuracy.

Statistical Analyses

For each bin of connections, a vector of 964 classification scores was obtained (one for each left out subject) and the classification score was thresholded at 0 (in the case of the strength/Euclidean distance bins, or at a threshold selected to optimize the area under a receiver operating characteristic curve for the case of the bins determined by *p*-values. Predicted diagnosis (autism vs. control) was compared to the actual diagnosis of each left out subject, and significant classification accuracy was determined by a binomial distribution. For 964 subjects, predicting 509 subjects (52.8%) correctly

corresponded to an uncorrected *p*-value of less than 0.05, and predicting 531 subjects (55.1%) correctly corresponds to *p*-value of less than 0.001. Two-proportion *z*-tests were used to test the following: 1) whether there was a group difference in the proportion of subjects with less than 50% of the BOLD volumes remaining after motion scrubbing (results found in the *BOLD Preprocessing section*), 2) whether classification accuracy differed between the eyes open and eyes closed subjects, 3) whether classification accuracy differed between the male and female subjects, and 4) whether accuracy increased when considering only those subjects with greater than 50% of the BOLD volumes remaining after motion scrubbing, rather than all 964 subjects. Two-sample *t*-tests were used to determine if there was a group difference in the number of remaining volumes (results above in *BOLD preprocessing section*).

Results

First, we investigated the overall accuracy, sensitivity, and specificity of the leave-one-out classifier for all 964 subjects in the ABIDE consortium (Figure 2.2) and the 16 data collection sites individually (Figure 2.3). For the entire ABIDE consortium, we achieved the highest overall accuracy (60.0%), sensitivity (62.0%), and specificity (58.0%) when connections were included in the classification algorithm if group differences for the connection met a *p*-value threshold of less than 10^{-4}; whereas the lowest accuracy (55.7%), sensitivity (57.1%), and specificity (54.4%) were found when all 26.4 million connections were included in the leave-one out classifier. When considering only those subjects with greater than 50% of the BOLD volumes remaining after motion scrubbing, the accuracy for the five different *p*-value thresholds increased

between 0.6% and 3.1%, although the difference was not significant compared to the accuracy for all 964 subjects ($p > 0.18$). No difference in classification accuracy was found between subjects who had their eyes open during the scan versus those who had their eyes closed, after correcting for multiple comparisons using an FDR of $q < 0.05$. Also, no difference in classification accuracy was found between male and female subjects, after correcting for multiple comparisons using an FDR of $q < 0.05$.

We also compared the accuracy, sensitivity, and specificity across sites using different *p*-value thresholds for determining which connections to include in the leave-one-out classifier. The accuracy, sensitivity, and specificity varied at each site depending on the *p*-value threshold, however, we consistently achieved the highest accuracy at Social Brain Lab (SBL; mean accuracy = 69.3%), Utah School of Medicine (USM; mean accuracy = 69.1%), Stanford (mean accuracy = 67.7%), and Pitt (mean accuracy = 65.4%); the highest sensitivity at San Diego State University (SDSU; 90.0%), Leuven (88.9%), SBL (84.0%), and Stanford (74.4%); and the highest specificity at USM(79.5%), Olin (75.0%), University of California-Los Angeles (UCLA; 71.5%), and Kennedy Krieger Institute (KKI; 70.6%).

Next, we determined whether the site's sample size or the number of imaging volumes from a single run related to the site's classification accuracy (Figure 2.4). The number of imaging volumes was positively correlated with accuracy ($r = 0.55$, $p = 0.03$). If the number of imaging volumes postscrubbing was averaged across site, the relationship between number of imaging volumes and accuracy was no longer significant. Sample size did not correlate with site's classification accuracy ($r = 0.17$, $p = 0.53$).

We then determined which brain regions and connection characteristics accurately classified the ABIDE subjects. In Figure 2.5, the following brain regions (and the 7265 connections in which they were involved) resulted in the highest accuracy: parahippocampal and fusiform gyri, insula, medial prefrontal cortex, posterior cingulate cortex, Wernicke area, and intraparietal sulcus. In Figure 2.6, two clusters of bins resulted in the highest accuracy. The first cluster included bins with short-range (10-25 mm) and medium-strength connections ($0.3 < z < 0.5$). The second cluster included bins with long-range (100-125 mm) and medium-strength connections ($0.15 < z < 0.4$).

Finally, we investigated the relationship between the subject's classifier score and behavioral measures (Figure 2.7). Estimates of symptom severity ($r = 0.13$, $p = 0.01$), as measured by the autism diagnostic observation schedule-generic (ADOS-G) social + communication algorithm score, and SRS ($r = 0.17$, $p = 0.002$) positively correlated with the classifier score; however, symptom severity, as measured by the autism diagnostic interview-revised (ADI-R) verbal domain algorithm score ($r = -0.06$, $p = 0.30$) or social domain algorithm score ($r = -0.04$, $p = 0.51$), and performance IQ ($r = -0.03$, $p = 0.38$) did not correlate with the classifier score. Verbal IQ ($r = -0.07$, $p = 0.05$) and Vineland adaptive behavior composite score ($r = 0.17$, $p = 0.002$) negatively correlate with the classifier score. In other words, as social function (lower SRS score is indicative of better social function), verbal IQ, and daily living skills increased and current level of symptom severity decreased, a subject was more likely to be classified as a control.

Discussion

Functional connectivity MRI data from a set of 26.4 million "connections" per subject is able to successfully classify a subject as autistic or typically developing using a leave-one-out approach with an accuracy of 60.0% ($p<2.2 * 10^{-10}$), across a set of 964 subjects contributed from 16 different international sites. Overall specificity was 58.0% and overall sensitivity was 62.0%. Classification consisted of a weighted average of connections that used no information about the left out subject except for age, gender, site, and handedness. Using a weighted average of all 26.4 million connections resulted in a classification accuracy of 55.7% ($p = 0.00017$), with best accuracy (60.0%) achieved for a subset of connections that satisfied $p < 10^{-4}$ for a difference between autism and control among remaining subjects for each left-out subject. Classification scores significantly covaried with metrics of current disease severity including ADOS-G (as opposed to ADI-R, which incorporates disease severity at early ages), SRS, and verbal IQ metrics. Classification accuracy significantly improved in sites for which longer BOLD imaging times were used, but no relationship was found between number of subjects contributed by a site and classification accuracy.

Classification accuracy was lower in this multisite study despite its much larger sample size when compared with a prior study using similar methods from a single site (Anderson et al., 2011d). The prior study achieved approximately 80% accuracy, with 90% accuracy for subjects under 20 years of age in both a primary cohort and a replication sample of affected and unaffected individuals from multiplex families. Several reasons may explain this difference. Expanding a classifier to accommodate multisite data necessarily involves dealing with many additional sources of variance. The

pulse sequence, magnetic field strength, scanner type, patient cohort and recruitment procedures, scan instructions (eyes open vs. closed vs. fixation), BOLD imaging length, age distribution, gender differences, and population ethnicity all varied across sites. Each of these variables has the potential to decrease sensitivity and specificity of functional connectivity measurements for autism. Nevertheless, a multisite cohort helps test generalizability of the results across different samples, making it more likely that connections identified as discriminatory between autism and control reflect disease properties rather than particulars of a single dataset.

Classification accuracy in the multisite cohort varied with the subset of connections used to construct the classifier. This finding reflected a tradeoff between improved accuracy when using more connections with decreased accuracy when including less specific connections in the classifier. This result argues against a homogenous regional distribution of connectivity abnormalities in autism in favor of a heterogeneous spatial distribution of connectivity disturbances that involves specific brain regions. Analysis of brain regions most affected in abnormal connections herein confirms the findings of previous reports: areas of greatest abnormality included the insula, regions of the default mode network including posterior cingulate and medial prefrontal cortex, fusiform and parahippocampal gyri, Wernicke area (posterior middle and superior temporal gyrus), and intraparietal sulcus (Anderson et al., 2011d; Gotts et al., 2012). All of these regions correspond to functional domains that are known to be impaired in autism, including attention, language, interoception, and memory. We note that some of these regions are in brain areas with relatively high susceptibility artifact and sensitivity to changes in brain shape (such as the medial prefrontal cortex). However,

given the coherent distribution of the default mode network, we favor an interpretation of network-based differences attributable to autism rather than underlying structural or artifactual sources of these findings.

When interrogating subsets of connections from an independent dataset based on the Euclidean distance between ROIs and connection strength in a previous study, we found that the most informative connections consisted of typically strong connections between distant ROIs that were weaker in autism, and typically negatively correlated connections, that were less negative in autism (less anticorrelated; (Anderson, Ferguson, Lopez-Larson, & Yurgelun-Todd, 2011). In the current study, the connection bins based on strength and distance that showed greatest classification accuracy were not precisely the same connection bins found previously. Rather, they were adjacent to the bins in the previous study. This is the case because the classification algorithm in the current study takes advantage of larger numbers of connections. There was again a tradeoff between using more connections, given that individual connections exhibited relatively little information, and using sets of connections that differed more in autism. Thus, bins of medium strength connections ($0.3<z<0.5$) outperformed the more specific bins of stronger connections ($z>0.5$) because the slightly weaker sets of connections included many more connections in the bin. This cautionary finding is relevant when attempting to identify the "optimal" set of connections for constructing candidate brain imaging biomarkers for ASD. Although specific affected regions appear to have autism connectivity abnormalities, classification schemes using only a small number of connections are likely to suffer from the high variance in metrics for individual connections.

This point is reinforced by a significant positive relationship between classification accuracy across sites and the length of BOLD imaging time per subject. Previous studies of test-retest reliability using functional connectivity MRI have shown that accuracy of results varies with one over the square root of BOLD imaging time (Anderson, Ferguson, Lopez-Larson, & Yurgelun-Todd, 2011c; Van Dijk et al., 2010), with only moderate reproducibility when short BOLD imaging times such as 5 minutes are used (Anderson et al., 2011c; Shehzad et al., 2009; Van Dijk et al., 2010). This relationship would suggest that classifiers using information from many brain regions continue to show benefit from much longer imaging times, with continued improvements even after hours of imaging across multiple sessions per subject to the extent this is practical (Anderson et al., 2011c; Anderson et al., 2013b; Greicius, Boyett-Anderson, Menon, & Reiss, 2004). Improvements in pulse sequence technology may also facilitate acquisition of greater numbers of volumes in shorter periods of time (Feinberg & Yacoub, 2012). The correlation between total imaging time and accuracy was more significant than the correlation between number of volumes used after scrubbing and accuracy. This might indicate that imaging time is more important than the number of volumes used. As multiband acquisition protocols become more prevalent (Setsompop et al., 2012), it will be important to determine the extent to which finer sampling versus longer imaging time will contribute to specificity of BOLD fcMRI measurements.

In a prior study that examined the effect of BOLD imaging time on ability to identify functional connectivity values obtained from a single individual compared to a group mean, individual “connections” could only be reliably distinguished after 25 minutes of BOLD imaging time. The number of connections that could be reliably

distinguished increased exponentially with imaging time for at least up to 10 hours of total imaging time (Anderson, Ferguson, Lopez-Larson, & Yurgelun-Todd, 2011b). Indeed, there is good theoretical basis that any desired accuracy can be obtained with sufficient imaging time, stretching into many hours. Although Van Dijk and colleagues report that the intrinsic connectivity measurements stabilize around 5 minutes of imaging time, they also state that noise continues to decrease at a rate of 1/sqrt(n), where n is the amount of imaging time (Van Dijk et al., 2010), which is in accordance with our findings (Anderson et al., 2011b). Moreover, they report that the stabilization is of composite network-level metrics rather than connections between small individual ROIs. In contrast, we have found that coarse network-level measurements are not particularly informative in classification compared to fine-grained metrics that take into account specific differences in the spatial distribution of connectivity. There may be no upper limit for continued improvements if more imaging time were obtained.

We found significant relationships between the classification score and some behavioral measures, such as social function and daily living skills; however, the proportion of variance in the behavioral measures that was explained by the linear relationship between the classification score and the behavioral measure was small (between 0.5% and 2.9%). This may be due to the overall poor accuracy of the classification approach. As accuracy and techniques for combining multisite data improves, we also expect an increase in the proportion of variance accounted for by the correlations.

Additional benefits may be achieved through improved classification algorithms that take advantage of machine learning techniques to allow more effective weighted

combinations of connections. Similarly, multimodal classifiers remain a promising, relatively untapped method for characterizing diagnostic and prognostic information about autism. Given classification accuracies of single site datasets exceeding 80% for structural MRI (Calderoni et al., 2012; Ecker et al., 2010a; Ecker et al., 2010b; Jiao et al., 2010; Sato et al., 2013; Uddin et al., 2011), diffusion tensor MRI (Ingalhalikar et al., 2011; Lange et al., 2010a), positron emission tomography (Duchesnay et al., 2011), and magnetoencephalography (Khan et al., 2013; Roberts et al., 2011; Roberts et al., 2010; Tsiaras et al., 2011), it would be of great interest to determine whether different modalities identify similar cohorts of subjects correctly, and whether a combination neuroimaging approach that leverages these different features might be able to achieve even greater accuracy than any one alone.

Although multisite datasets such as those in ABIDE are invaluable for testing replicability of neuroimaging findings in autism, they contain inherent limitations that should be recognized. Large inhomogeneities in acquisition parameters, subject populations, and research protocols limit the sensitivity for detecting abnormalities. These inhomogeneities may overwhelm the ability of discriminating many findings, and may lead to overconfidence in a result as definitive because of the large sample of subjects used. There remains a need for replicating results in high-quality, carefully controlled individual datasets that may show increased sensitivity for some results compared to multisite data, as exhibited by classification accuracy in the present study. Preprocessing methods may also bias results in unpredictable ways, as has been suggested with head motion correction strategies (Power et al., 2012; Van Dijk, Sabuncu, & Buckner, 2012) and regression procedures (Anderson et al., 2011a; Murphy, Birn,

Handwerker, Jones, & Bandettini, 2009; Saad et al., 2012). Datasets such as those in ABIDE will be of great value in testing multiple procedural manipulations in relatively large samples allowing determination of optimal processing methods for specific questions. Ultimately, it is unknown whether differences in resting state functional connectivity in autism arise from differential performance of the "resting" task or underlying differences in structural connectivity reflected in the measurements. Continuing comparison with structural metrics such as diffusion tensor imaging will help to clarify this point.

Nevertheless, it remains an attractive hypothesis that with longer imaging times, controlled acquisition strategies, integration of multimodal features, and improvement in classification methodology, neuroimaging may be able to contribute useful biological information to the clinical diagnosis and care of individuals with autism spectrum disorders and further elucidate pathophysiology and brain-based intermediate phenotypes.

Table 2.1. Subjects included from the ABIDE sample with demographic information.

	Age	ADI-R social	ADI-R verbal	ADOS-G total	Verbal IQ	Performance IQ	SRS total	Vineland
Number of subjects	964	348	349	348	781	796	335	201
Control	(426 M, 91 F)	0	0	32	413	425	160	80
Autism	(396 M, 51 F)	348	349	316	367	371	175	121
Control mean +/- s.d.	16.9 +/- 7.56	NA	NA	1.25 +/- 1.37	112 +/- 13.3	108 +/- 13.3	21.2 +/- 16.2	105 +/- 11.6
(Control range)	(6.47 - 56.2)	NA	NA	(0 - 4)	(67 - 147)	(67 - 155)	(0 - 103)	(77 - 131)
Autism mean +/- s.d.	16.6 +/- 8.1	19.7 +/- 5.65	15.9 +/- 4.55	11.9 +/- 3.81	105 +/- 17.4	106 +/- 17.2	91.6 +/- 30.6	75 +/- 13.2
(Autism range)	(7 - 64)	(2 - 30)	(2 - 26)	(2 - 22)	(50 - 149)	(59 - 157)	(6 - 164)	(41 - 106)

Figure 2.1. Summary of classification approach. Step 1: Association matrices corresponding to the intrinsic connectivity between each pair of 7266 gray matter regions (about 26.4 million connections) are estimated for the left out subject and the 963 remaining subjects. Step 2: Plot depicting an example connection (i.e., single cell of the possible 26.4 million cells from the association matrices in Step 1) for the 964 subjects. The plot includes axes for correlation strength and age; however, the plot represents a multidimensional space that includes age-squared, gender, and handedness as covariates. *Black line*, fit line for the control group; *red line*, fit line for the autism group; *green data point*, left out subject (a control subject in this example); *green X,* estimated value for the control group; *blue X*, estimated value for autism group; *green vertical line*, difference between actual connection strength value for left out subject and estimated value for control group; *blue vertical line*, difference between actual connection strength value for left out subject and estimated value for autism group. Steps 3 and 4 are described in the text.

Step 1: Create functional connectivity association matrices for 964 subjects and leave out a single subject.

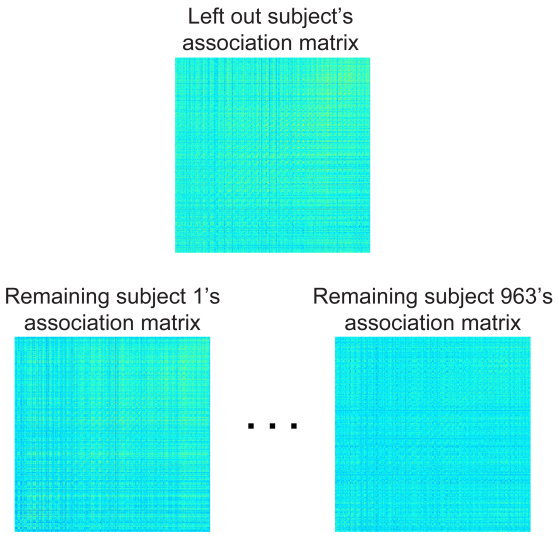

Step 2: General linear model was fit for autism and control groups separately. Differences between the left out subject's value and the autism and control group estimated values were calculated.

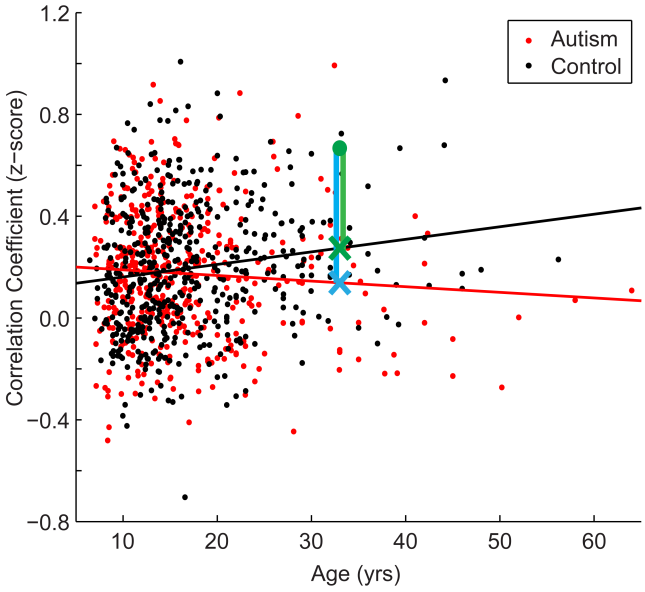

Step 3: The difference (i,.e., | Left Out - Autism | - | Left Out - Control |) was added to the running total for the subject for each binning scheme including the connection.

Step 4: Repeat steps 1-3 for all 26.4 million connections one at a time and for all 964 subjects, leaving one subject out at a time, until classifier score is totaled for each subject.

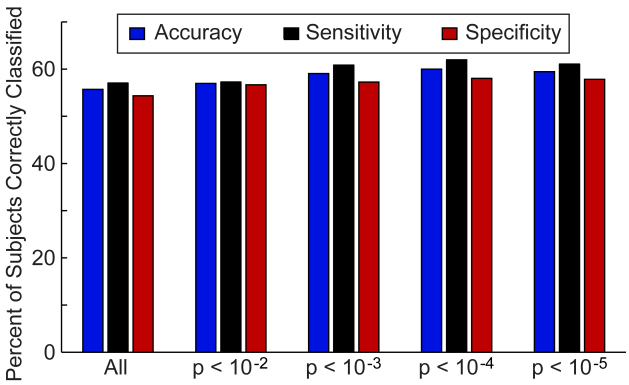

Figure 2.2 Total accuracy, sensitivity, and specificity for leave-one-out classifier in 964 subjects. The total accuracy, sensitivity, and specificity are shown when all 26.4 million connections were included in the classifier and then for different *p*-value thresholds that determine which connections are included in the classifier.

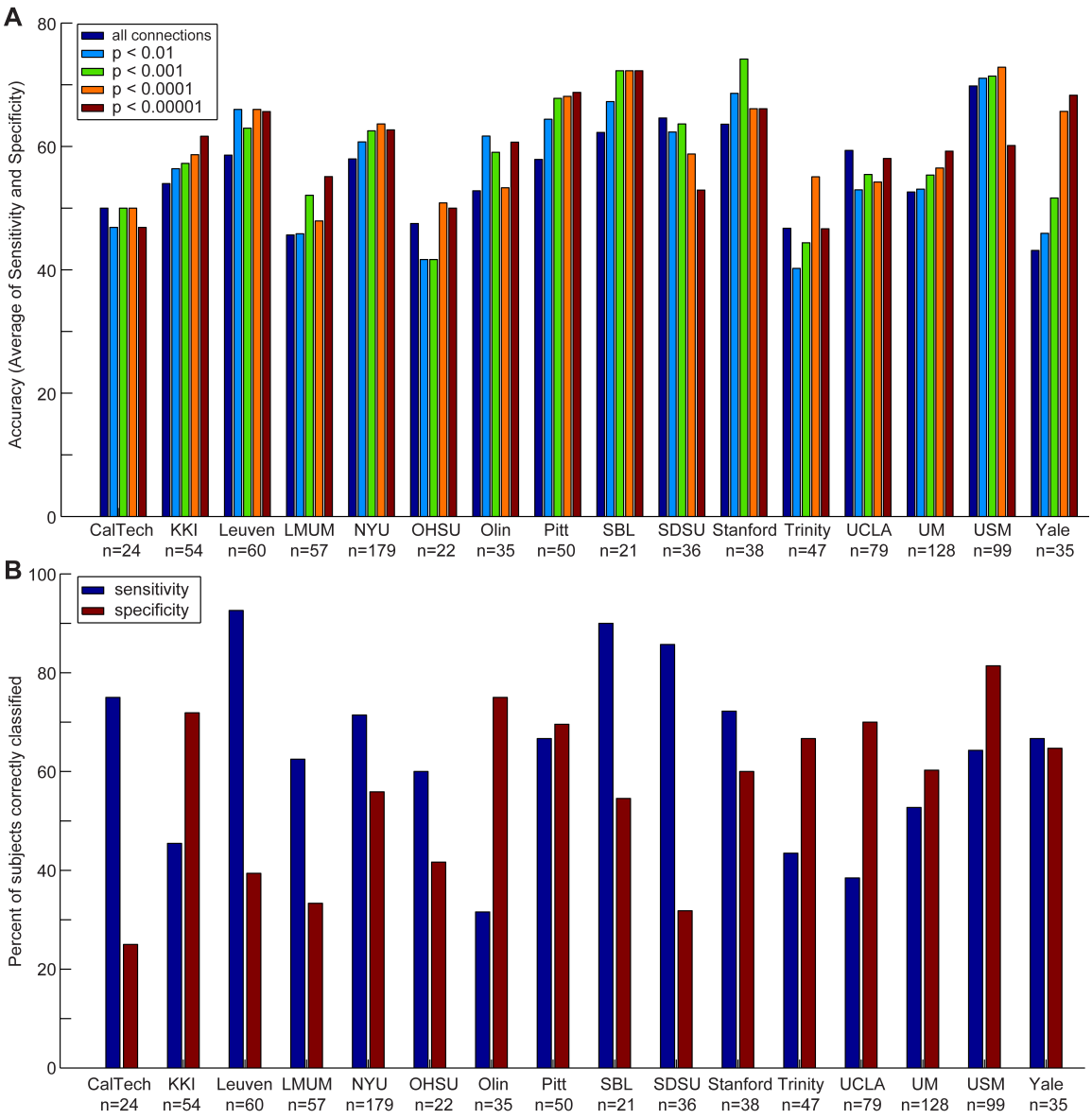

Figure 2.3. Accuracy, sensitivity, and specificity for each data acquisition site. Accuracy (A) is shown for each data acquisition site at different *p*-value thresholds. The sensitivity and specificity (B) are shown for each data acquisition site at a threshold of $p < 0.0001$ (i.e., the threshold at which optimal total accuracy was obtained in Figure 2.2).

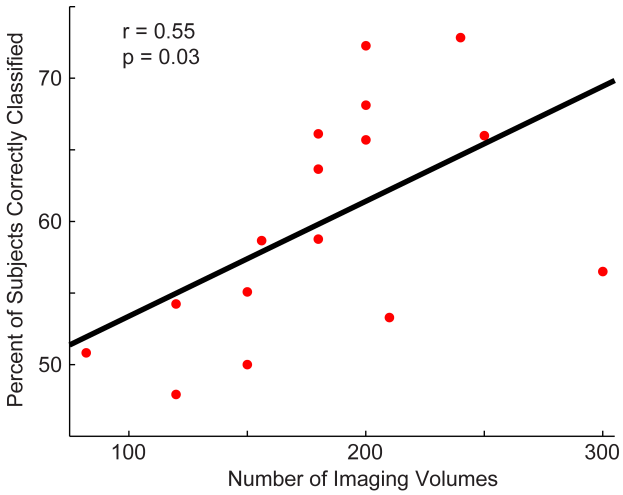

Figure 2.4. Relationship between a site's total accuracy and the number of imaging volumes acquired by each site. Each site's total accuracy was calculated when using a $p<$ 0.0001 threshold (i.e., the threshold at which optimal total accuracy was obtained in Figure 2.2) and correlated with the number of BOLD imaging volumes acquired during the resting-state sequence.

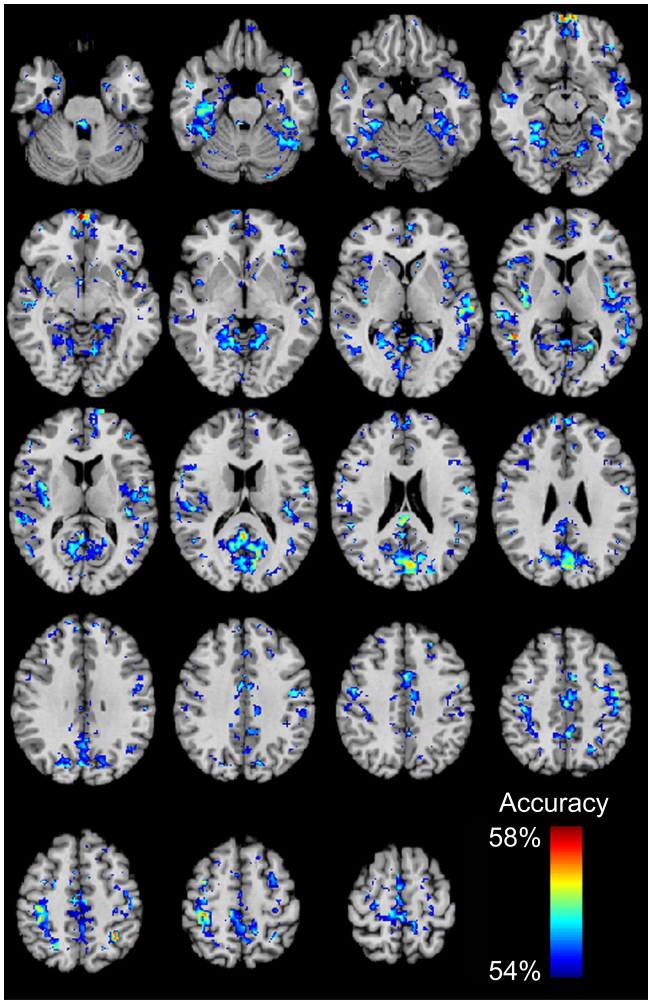

Figure 2.5. Total accuracy for 7266 brain regions. Accuracy was determined for each of the 7266 brain regions independently by only taking into account the 7265 connections in which a given region was involved (no *p*-value threshold, all connections used). The minimum accuracy displayed for a single region is 53.95%, which was the false discovery rate corrected percentage for 7266 regions and a binomial cumulative distribution.

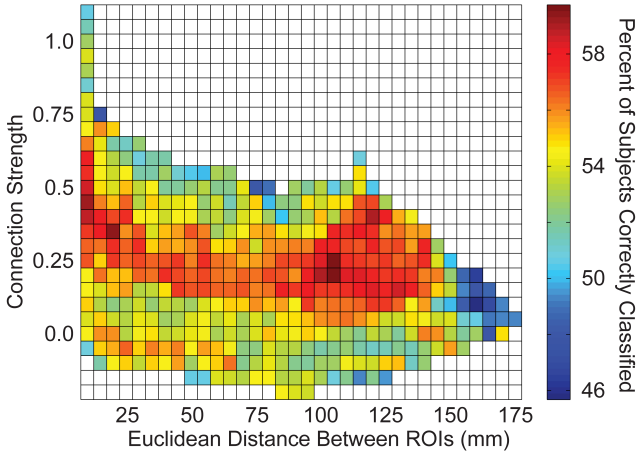

Figure 2.6. Total accuracy across connection strength and distance between brain regions. The 26.4 million connections were divided up into bins based on the correlation strength of the connection (determined by an independent sample) and the distance between the connection's two endpoints. Accuracy is displayed for each bin with at least one connection.

Figure 2.7. Scatterplots of relationships between classifier scores and behavior. Scatterplots depict the relationship between the classifier scores for control subjects (*black*) and subjects with autism (*red*) and the following behavioral measures: ADOS-G social + communication algorithm score (A), ADI-R social verbal algorithm score (B), verbal IQ (C), performance IQ (D), SRS total score (E), and Vineland adaptive composite standard score (F). Correlation coefficients and corresponding *p*-values are included on the plots.

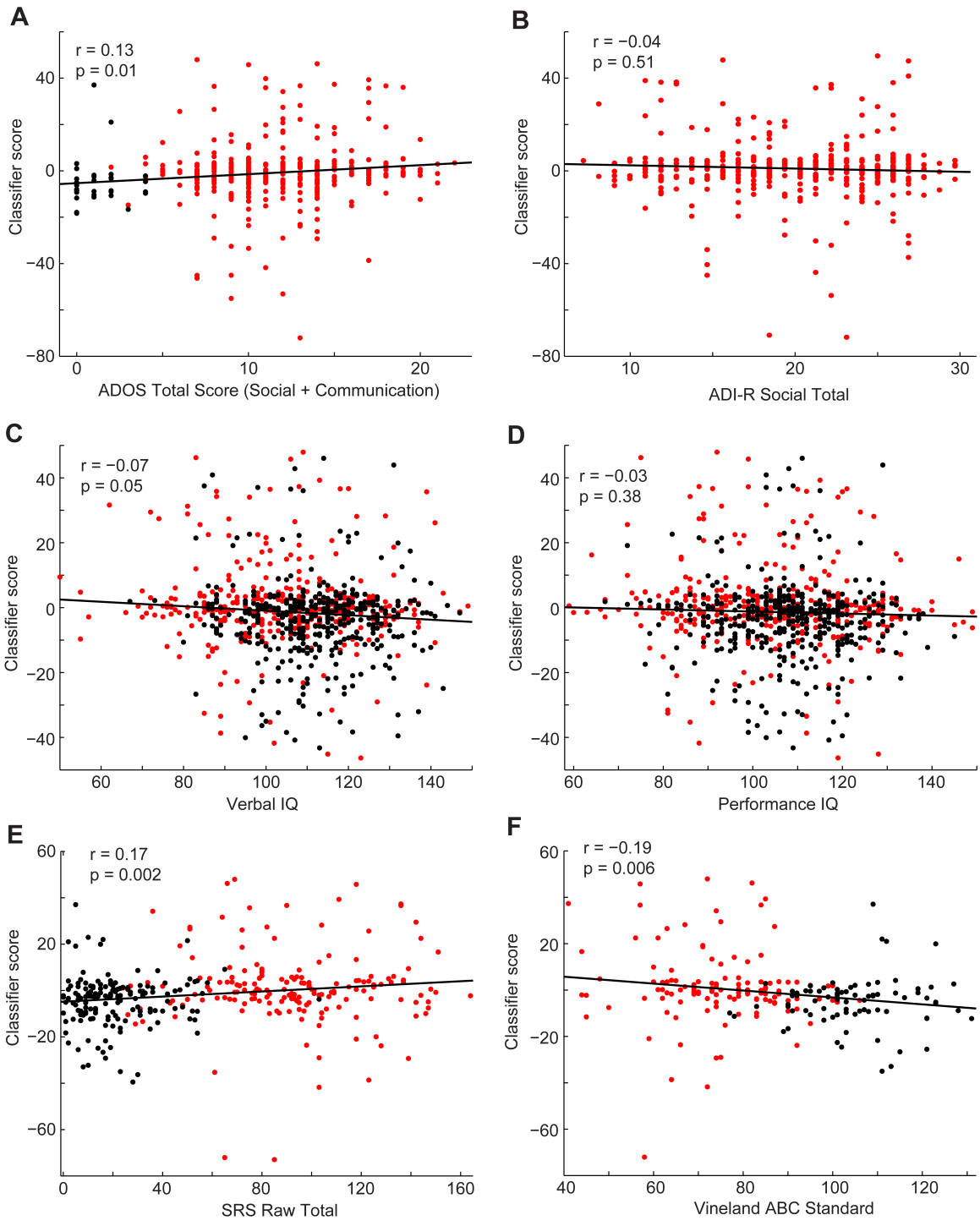
A
r = 0.13
p = 0.01
Classifier score
ADOS Total Score (Social + Communication)
B
r = −0.04
p = 0.51
Classifier score
ADI-R Social Total
C
r = −0.07
p = 0.05
Classifier score
Verbal IQ
D
r = −0.03
p = 0.38
Classifier score
Performance IQ
E
r = 0.17
p = 0.002
Classifier score
SRS Raw Total
F
r = −0.19
p = 0.006
Classifier score
Vineland ABC Standard

CHAPTER 3

AN EVALUATION OF THE LEFT-BRAIN VERSUS RIGHT-BRAIN HYPOTHESIS WITH FUNCTIONAL CONNECTIVITY MAGNETIC RESONANCE IMAGING

Lateralized brain regions direct functions such as language and visuospatial processing. In most right-handed individuals, paying attention to stimuli involving language elicits brain activity lateralized to the left hemisphere, whereas paying attention to stimuli involving visuospatial processing elicits brain activity lateralized to the right hemisphere (Herve, Zago, Petit, Mazoyer, & Tzourio-Mazoyer, 2013; Shulman et al., 2010; Stephan et al., 2003; Toga & Thompson, 2003). Atypical lateralization in brain structure and function is associated with neuropsychiatric disorders such as autism spectrum disorders and schizophrenia (Chance, Casanova, Switala, & Crow, 2008; Fletcher et al., 2010; Herbert et al., 2002; Kleinhans, Muller, Cohen, & Courchesne, 2008a; Lange et al., 2010b; Oertel-Knochel & Linden, 2011), although there is considerable variation within typically developing individuals in the strength to which specific functions such as language are lateralized to the canonical side, particularly for left-handed and ambidextrous individuals (Szaflarski et al., 2002).

Previous studies of brain laterality are largely limited to regional assessment of specialized functions and differences in structural lateralization. It has been well

documented that small structural asymmetries consisting of a frontal (right>left) and occipital (left>right) shear effect are present in most individuals (LeMay, 1977), in addition to asymmetries of the planum temporale, angular gyrus, caudate, and insula (Watkins et al., 2001). A diffusion tensor study of a predefined brain parcellation using graph-theoretical methods showed increased efficiency and connectedness within the right hemisphere, but with regions of greatest network centrality in the left hemisphere (Iturria-Medina et al., 2011). Additional asymmetries in gray matter volume have been observed within nodes of the default mode network (Saenger, Barrios, Martinez-Gudino, & Alcauter, 2012).

With the recent development of resting state functional connectivity magnetic resonance imaging (rs-fcMRI) techniques, it has become possible to characterize whole-brain lateralization using a data-driven approach. Two recent studies have investigated whole-brain lateralization using rs-fcMRI (Liu, Stufflebeam, Sepulcre, Hedden, & Buckner, 2009; Tomasi & Volkow, 2012b). Liu et al. (2009) found that connectivity of classical language regions, medial prefrontal cortex, and posterior cingulate cortex was most strongly left-lateralized, whereas that of insula, angular gyrus, anterior cingulate cortex, and visual cortex was most strongly right-lateralized. Males had more strongly lateralized connections than females. In a factor analysis, the four factors that accounted for the most variance involved regions from the following cortical networks: visual, default, salience, and language. Handedness influenced the laterality of the four factors; however, it affected laterality differently across the factors.

Tomasi and Volkow (2012) demonstrated that short- and long-range connections were predominantly right-lateralized in brain regions surrounding the lateral sulcus,

whereas left-lateralized connections were limited to medial areas of the occipital cortex and superior rim of the parietal and posterior frontal lobes (Tomasi & Volkow, 2012b). Additionally, much of the medial aspect of the frontal and parietal lobes had right-lateralized long-range connections, whereas Broca area and angular gyrus had left-lateralized long-range connections. As in Liu et al. (2009), males had more lateralized connections than females, although the effect was small.

These studies raise important questions. Does functional connectivity lateralization reflect structural asymmetry or does it represent a lateralized difference in the strength of synaptic connections? Does a whole-brain phenotype of relatively greater "left-brain" or "right-brain" functional specialization across individuals exist, or are lateralized connections in different brain networks independent of each other within an individual? Are these connectivity patterns modified with age, as the brain matures into an adult phenotype? In this manuscript, we address these questions and find that lateralized regions create left- and right-lateralized networks, lateralized connections are independent from one another across individuals, and that the majority of functional lateralization occurs before age 7.

Materials and Methods

Publicly Released Datasets – 1011 subjects

One thousand and eleven subjects were analyzed from publicly available datasets released with the open-access 1000 Functional Connectomes Project (http://fcon_1000.projects.nitrc.org/) in which resting-state functional magnetic resonance imaging (fMRI) scans have been aggregated from 28 sites (Biswal et al., 2010)

as well as typically developing subjects from the ADHD 200 project from the International Neuroimaging Data-sharing Initiative (fcon_1000.projects.nitrc.org/indi/adhd200/index.html) including 8 sites (ADHD-200_Consortium, 2012). For inclusion we required that subjects' ages were between 7 and 29, with BOLD whole-brain coverage from Montreal Neurologic Institute (MNI) coordinates z=-35 to z=70. Any subject for whom preprocessed data did not cover all 7266 regions of interest (ROIs) used for this analysis was discarded prior to analysis (see Anderson et al. (2011) for a list of the MNI coordinates for the 7266 ROIs). Also for inclusion, all subjects included an MPRAGE anatomic sequence that was successfully segmented and normalized to MNI space. Although preprocessing steps were performed using an automated batch script, the results of normalization, segmentation, and realignment steps were manually inspected for all subjects, and any subject for whom the normalized and segmented images were not in close alignment with the MNI template on visual inspection were discarded. The datasets from which subjects met all criteria are listed in Table 3.1. The mean age of all subjects was 18.3 +/- 5.6 s.d. years (range 7-29). 587 subjects were male; 424 were female. All subjects were processed in the same manner regardless of the site from which they were obtained.

Gray Matter Density Measurements and Structural Lateralization Metric

Gray matter density images were created by normalizing and segmenting MPRAGE images using SPM8 (Wellcome Trust, London) into three tissue classes representing gray matter, white matter, and cerebrospinal fluid (CSF). Smoothly varying intensity changes as well as artifactual intensity alterations as a result of the

normalization step were corrected for using a standard modulation algorithm within SPM. We then derived mean gray matter intensities within 7266 spherical (5 mm radius) seed ROI (Anderson, Ferguson, Lopez-Larson, & Yurgelun-Todd, 2011; Anderson et al., 2011d; Ferguson & Anderson, 2012) that formed a lattice covering the gray matter.

Segmented gray matter images from the normalized MPRAGE images were also flipped across the midsagittal plane, and the difference in mean gray matter density was recorded for each ROI as the structural lateralization index ([unflipped density - flipped density]/ [unflipped density + flipped density]).

fMRI Preprocessing

The following sequence was used for image preprocessing of all blood oxygen level-dependent (BOLD) image datasets. Using SPM8 toolbox (Wellcome Trust, London), BOLD images were realigned (realign, estimate and write), coregistered to MPRAGE image (coregister, estimate and write), and the MPRAGE image (with coregistered BOLD images) was normalized to an MNI template with spatial resolution of 3 mm^3 voxels (normalize, estimate and write, T1.nii template). Gray matter, white matter and CSF were segmented from MPRAGE images using SPM8 segment function (modulated, normalized, thorough clean). Images were bandpass filtered between 0.001 and 0.1 Hz and a linear detrend was performed at each voxel in the brain. The lower limit of 0.001 Hz was chosen in order to be certain as much neural information was included as possible (Anderson et al., 2013c). The linear detrend removed much of the contribution of low frequencies given the relatively short time series available in the dataset. Time series were averaged from two ROIs in the white matter (bilateral centrum

semiovale), CSF (lateral ventricles), soft tissues of the head and face, and six rigid motion correction parameters from the realignment step as previously described and for each voxel (Anderson et al., 2011d), a general linear model was used to find a best fit for white matter, CSF, soft tissues, and motion parameter time series, which were subtracted from the voxel's time series. No regression of the global signal was included. No smoothing was performed to avoid contaminating the signal near the midsagittal plane. Recent reports have highlighted the necessity to take extra precaution when dealing with motion artifact (Power et al., 2012; Satterthwaite et al., 2013; Van Dijk et al., 2012). Therefore, a motion scrubbing procedure was implemented that involved removing frames with root-mean-square motion parameters > 0.2 mm prior to analysis of connectivity results (Power et al., 2012).

Functional Lateralization Metric

Functional correlation was obtained as the Fisher-transformed Pearson correlation coefficient between each pair of the 7266 ROIs within the same hemisphere. We only analyzed connections within a single hemisphere and the opposite hemisphere homologues because of ambiguity of "lateralization" of a cross-hemisphere connection. Preprocessed images were inverted across the midsagittal plane, and analogous Fisher-transformed correlation coefficients were obtained between each pair of the same ROIs on the flipped images. Functional lateralization index was defined as the difference (unflipped - flipped) between Fisher-transformed correlation coefficients. The functional lateralization index did not include the normalization term in the denominator like the structural lateralization index or that is commonly used in functional lateralization studies

(Seghier, 2008) because the functional connectivity correlations include positive and negative values rather than strictly positive values. The use of a denominator when calculating a functional lateralization index may result in index values with a discontinuity in the denominator, binary index values (e.g., if flipped = -0.01 and unflipped = +0.01, then [unflipped – flipped] / [|unflipped| + |flipped|] = 1), or index values that accentuate small differences in laterality (e.g., if flipped = 0.01 and unflipped = 0.03, then [unflipped – flipped] / [|unflipped| + |flipped|] = 0.5). Moreover, the functional correlation measurements already occupy the interval between -1 and 1.

The structural effects were regressed out of the functional lateralization metrics. For each of the 7266 ROIs, the structural lateralization indices (Figure 3.1) calculated for the given ROI and the other 7265 ROIs were regressed from the corresponding functional lateralization indices on a subject-by-subject basis using a general linear model (glmfit.m in MATLAB). More specifically, for a connection involving two ROIs, the mean structural lateralization index for the two ROI endpoints was used as a regressor, with regression performed across the set of all connections for an individual subject. Most of the structural/functional correlation was removed after regression, although a residual relationship remains. These data indicate that even after accounting for subject-to-subject variation in structural asymmetries, nodes that show more gray matter in one hemisphere tend to have stronger functional connections involving that node in the same hemisphere.

After regression, significantly lateralized connections were those for which a two-tailed *t*-test showed values that were different from 0 after correction for multiple comparisons using acceptable false discovery rate of $q<0.05$. Sparse binarized graphs of significantly left- and right-lateralized connections were obtained and the degree was

calculated as the sum of all significantly left- or right-lateralized connections in which a given node is represented. Hubs were defined as local maxima in the images of degree of the left- and right-lateralized graphs (Table 3.2 and Figure 3.2). In neuroimaging literature, it is common to refer to hubs as brain regions that are highly connected, either structurally or functionally, to other brain regions and play a central role in brain network dynamics (Achard, Salvador, Whitcher, Suckling, & Bullmore, 2006; Buckner et al., 2009; Sporns, Honey, & Kotter, 2007). In this manuscript, we take that definition one step further by referring to hubs as brain regions that are involved in many lateralized functional connections. Thus, "hubs" need not represent nodes of intrinsic connectivity networks. Large changes in degree were seen with structural regression compared to without structural regression in the occipital pole, medial posterior insula, caudate, putamen, thalamus, and lingual gyrus adjacent to the occipital horn of the lateral ventricle. These regions were not considered hubs in subsequent analyses since there was likely a large effect of structural asymmetry on lateralization. We identified 9 remaining hubs in the left-lateralized graph and 11 hubs in the right-lateralized graph. We ensured that all 9 left-lateralized hubs and 11 right-lateralized hubs, respectively, were at least 10 mm apart from one another. Two of the left hubs were within 10 mm of the interhemispheric homologues of two of the right hubs (Broca area and Broca homologue and left and right supplementary motor area), meaning the areas participate in strongly lateralized connections in both hemispheres.

Statistical Analyses

All statistical analyses were performed in MATLAB using MATLAB's statistical toolbox. Each cortical hub's lateralization pattern with other hubs in the ipsilateral hemisphere of the cerebral cortex was determined by performing one-sample *t*-tests on the functional connections involving the cortical hub as the seed and the other ipsilateral hubs. Global versus local lateralization was tested by calculating a functional lateralization index for connections involving right-hemispheric hubs (i.e., 11 right-hemispheric hubs resulting in 55 pairwise connections) and connections involving left-hemispheric hubs (i.e., 9 left-hemispheric hubs resulting in 36 pairwise connections) for each subject and then covarying each connection with all other connections across subjects for a total of 4095 pairs of 91 connections. This effectively asks whether two connections, each between hubs in one hemisphere, tend to be relatively stronger in the same subjects. To test for gender effects, two-sample *t*-tests were applied to 1) the average left and right functional laterality index values for each subject and 2) on the set of connections involving the 20 lateralization hubs (total of 195 comparisons). To test the effects of age, correlations were measured for 1) the average left and right functional laterality index values for each subject and 2) the set of connections involving the 20 lateralization hubs (total of 195 correlations).

To test whether the results from a single site corresponded with overall results, the mean functional laterality indices for the Beijing (site with largest sample size) subjects were correlated with the mean functional laterality indices for all other subjects. To test if excessive noise was introduced by including sites with small samples (i.e., < 10 subjects), the mean functional laterality indices excluding the 23 subjects from sites with small

samples were correlated with the mean functional laterality indices for all subjects. Spearman correlations (because of the non-Gaussian nature of the data) were used to test whether there was any relationship between functional lateralization index of the 91 connections involving intrahemispheric hubs and the following movement measurements: mean movement during scan, maximum movement from one frame to the next, the number of frames discarded during the scrubbing procedure described above, and the percent of frames discarded during the scrubbing procedure. All analyses in this manuscript that involved more than a single test included a correction for multiple comparisons using a false discovery rate of $q < 0.05$.

Results

We first investigated each cortical hub's lateralization pattern across the ipsilateral hemisphere of the cerebral cortex. The lateralization pattern consisted of two parts (Figure 3.3). First, the left-lateralized connections included regions from the default mode network (medial prefrontal cortex, posterior cingulate cortex, temporoparietal junction, and inferior temporal cortex) and classical language regions (Broca area and Wernicke area). Second, the right-lateralized connections included regions that can be broadly categorized as attentional areas (frontal eye fields, middle temporal area (area MT), anterior cingulate cortex, insular cortex, supplementary motor area, intraparietal sulcus, superior parietal lobules, and dorsolateral prefrontal cortex). The lone exception among the left-hemispheric hubs, the medial prefrontal cortex, shared right-lateralized connections with much of the typically left-lateralized surrounding cortex and the posterior cingulate cortex. Among the right-hemispheric hubs there were two patterns:

hubs that were right-lateralized to the default mode network (and all other right-hemispheric hubs), and hubs that were left-lateralized to default mode network (but right-lateralized to the right-hemispheric hubs). Nevertheless, some of the hubs that were right-lateralized (such as lateral IPS) to all 20 hubs show extensive left-lateralized connections to nonhub regions, indicating that lateralization networks have hub-specific features.

The laterality of connections between the 20 hubs is summarized in Figure 3.4. Colored squares indicate connections where the functional lateralization index, after regression of the structural lateralization index across subjects, was significantly left or right lateralized after FDR correction for multiple comparisons across all possible connections among the 20 hubs. When comparing the laterality between interhemispheric connections (i.e., connection involving a left-lateralized hub and a right-lateralized hub), the functional lateralization index was calculated by flipping the right-lateralized hub across the midsagittal plane into the left hemisphere in order to maintain intrahemispheric comparisons. Connections between left-hemispheric hubs were almost entirely left-lateralized, and connections between right-lateralized hubs were almost entirely right-lateralized. Although the hubs were selected for having a high degree in the graph of significantly lateralized connections, this did not require the hubs to all show consistent lateralization with each other and suggests that the left-hemispheric hubs and right-hemispheric hubs form a backbone of two broader lateralized networks in the brain, one in the left hemisphere and one in the right hemisphere.

Next, we determined whether lateralization was a whole brain or a local property. In other words, if connections between left-hemispheric hubs were strongly left-lateralized in a subject, did this correspond to connections among right-hemispheric hubs

showing stronger right lateralization? Figure 3.5 summarizes the results. Of the 630 comparisons involving left-hemispheric hubs, only one (0.2%) showed significant negative correlation (i.e., as one connection between left-hemispheric hubs became more left-lateralized the other connection between left-hemispheric hubs became less left-lateralized), whereas 144 significant comparisons (22.9%) involved positively correlated connections. Of the 990 comparisons involving right-hemispheric hubs, none negatively correlated and 329 comparisons (33.2%) involved positively correlated connections. Almost all of the significant positively correlated connections (left: 141/144; right: 314/329) included connections with a common hub. Of the 1620 comparisons involving right-hemispheric hub connections versus left-hemispheric hub connections, 20 were significantly negatively correlated (1.2%) and 16 are significantly positively correlated (1.0%). The majority of the significant negatively correlated connections (16/20) and significant positively correlated connections (8/16) included connections with a right-hemispheric hub that when flipped across the midline is <10 mm from a left-hemispheric hub.

Together, these results imply lateralization is a local property rather than a whole-brain property. If a hub formed a strongly lateralized connection with another ipsilateral hub in a subset of subjects, it was more likely that the same hub would form strongly lateralized connections with other ipsilateral hubs in those subjects. But with rare exceptions, no effect was seen between other distinct ipsilateral hubs in the same subjects.

We investigated the effects of gender on lateralization and how lateralization changes over development between the ages of 7 and 29. No significant gender effects

were found when testing the mean lateralization for the connections involving left- and right-hemispheric hubs, respectively, or a subset of connections between the 20 hubs. We found small, significant relationships between age and mean lateralization for the connections involving left- and right-hemispheric hubs, respectively (Figure 3.6; left: r = 0.08 p = 0.009; right: r = 0.09 p = 0.004). Because there was a significant effect, albeit small, when averaging across all connections between left-hemispheric or right-hemispheric hubs, we extended our analysis to the individual left hub-left hub and right hub-right hub connections. Table 3.3 lists the ten right-lateralized connections that become significantly more right-lateralized across development and survive correction for multiple comparisons using a false discovery rate of $q < 0.05$.

Finally, we tested whether the results described were reproducible in a smaller sample and whether they were due to potential confounds. We compared the relationship between mean functional lateralization of the 91 connections involving intrahemispheric hubs from the Beijing site, the site with the largest sample size, and the mean from all other sites. The measurements between the two subsamples corresponded highly (r = 0.85, p = 2.3 e -26). We also determined that including sites with small samples (5 sites with less than 10 subjects for a total of 23 subjects) did not introduce excessive amounts of variability (Figure 3.7B) and that the lateralization results were not due to head motion artifact. The mean functional lateralization of the 91 connections involving intrahemispheric hubs was virtually identical when including subjects from sites with small samples (Figure 3.7B; r = 0.999, p = 7.9 e -128). No relationship between the functional lateralization index of the 91 connections involving intrahemispheric hubs and the single-subject motion measurements (e.g., mean movement, the number of frames

discarded during the scrubbing procedure described above, etc.) survived multiple comparison correction (false discovery rate of $q < 0.05$).

Discussion

By comparing the magnitude of functional connectivity in a large multisite cohort (n=1011) of subjects, we demonstrate that a left-dominant network and a right-dominant network can be defined in which discrete hubs show consistent lateralization among connections between the respective left- and right-hemispheric hubs. The identified left-dominant and right-dominant hubs correspond well to known architecture of intrinsic connectivity networks, and show persistent lateralization of connectivity even after removal of the variance attributed to structural asymmetry of gray matter. We also demonstrate that lateralization is a local rather than a whole-brain property. In other words, when a connection of interest is strongly lateralized, the degree of lateralization for the other connections throughout the brain relates only in the connections that have a hub in common with the connection of interest.

Our data are broadly consistent with previous studies regarding the spatial distribution of lateralization of functional connectivity (Liu et al., 2009; Tomasi & Volkow, 2012b). We find that brain regions showing consistently strong left-lateralization include classical language regions (Broca area, Wernicke area, lateral premotor, and anterior supplementary motor areas). MNI coordinates associated with greatest left-lateralization match closely those reported in task-based fMRI studies of language (Anderson et al., 2010). Broca and Wernicke areas have been shown to comprise a distributed language network, predominantly left-lateralized, in their

functional connections and include both adjacent cortical as well as subcortical regions (Tomasi & Volkow, 2012a).

Other left-lateralized hubs include core regions of the default mode network (posterior cingulate, medial prefrontal, temporoparietal junction (Raichle et al., 2001). In a diverse assortment of cognitive tasks (Gusnard & Raichle, 2001), this network shows greater activity during the resting state than during the task (Mayer, Roebroeck, Maurer, & Linden, 2010), and it has been proposed that this network may be involved in attending to internal stimuli, internal narrative, or self-reflection (Andrews-Hanna, Reidler, Huang, & Buckner, 2010; Cavanna & Trimble, 2006; Gusnard, Akbudak, Shulman, & Raichle, 2001; Northoff et al., 2006). Recent evidence suggests this network may be comprised of a midline core active during self-referential thought, and a medial temporal core active during memory of past events (Andrews-Hanna, Reidler, Sepulcre, Poulin, & Buckner, 2010), with the precuneus showing three anterior/posterior subdivisions with differing connectivity patterns (Margulies et al., 2009).

In contrast, hubs of right-lateralized functional connectivity correspond well to canonical regions of the dorsal and ventral attention networks and the cingulo-insular or salience network (Dosenbach et al., 2007; Fox, Corbetta, Snyder, Vincent, & Raichle, 2006; Fox et al., 2005; Seeley et al., 2007; Yeo et al., 2011). This network is more active during tasks requiring attention to external stimuli or assessment of stimulus salience or novelty (Corbetta & Shulman, 2002; Seeley et al., 2007). Virtually all of the described hubs of this network show right lateralization to each other in our analysis, including intraparietal sulcus, frontal eye fields, area MT, anterior insula, and dorsolateral prefrontal cortex. Right lateralization of external stimulus attention is consistent with

lesion studies reporting much greater incidence of hemispatial neglect following right-hemispheric injury (Corbetta & Shulman, 2011; Sestieri, Corbetta, Romani, & Shulman, 2011), particularly associated with lesions to regions of the ventral attention network (Corbetta & Shulman, 2011).

In popular reports, "left-brained" and "right-brained" have become terms associated with both personality traits and cognitive strategies, with a "left-brained" individual or cognitive style typically associated with a logical, methodical approach and "right-brained" with a more creative, fluid, and intuitive approach. Based on the brain regions we identified as hubs in the broader left-dominant and right-dominant connectivity networks, a more consistent schema might include left-dominant connections associated with language and perception of internal stimuli, and right-dominant connections associated with attention to external stimuli.

Yet our analyses suggest that an individual brain is not "left-brained" or "right-brained" as a global property, but that asymmetric lateralization is a property of individual nodes or local subnetworks, and that different aspects of the left-dominant network and right-dominant network may show relatively greater or lesser lateralization within an individual. If a connection involving one of the left hubs is strongly left-lateralized in an individual, then other connections in the left-dominant network also involving this hub may also be more strongly left lateralized, but this did not translate to a significantly generalized lateralization of the left-dominant network or right-dominant network. Similarly, if a left-dominant network connection was strongly left lateralized, this had no significant effect on the degree of lateralization within connections in the

right-dominant network, except for those connections where a left-lateralized connection included a hub that was overlapping or close to a homotopic right-lateralized hub.

We observe that lateralization of uncorrected functional correlation measurements includes a significant effect from structural asymmetries such as gyral position. We attempted to correct for this effect by regressing out gray matter density across subjects for each of the endpoints of every connection in our dataset to obtain a less biased measurement of functional lateralization. Although this effect is difficult to completely remove, it is unlikely that the relationships we describe are wholly attributable to structural asymmetries. The map of gray matter density lateralization shows a different spatial distribution from the map of functional connectivity lateralization, with structural lateralization varying abruptly between left and right with each gyrus, and functional lateralization following well-known functional architecture of intrinsic connectivity networks. Two of the nodes are within 10 mm of their homotopic equivalents in the left- and right-dominant networks. Thus, the same hub is lateralized to one set of connections in the left hemisphere and to a different set of connections in the right hemisphere. This is consistent with prior diffusion tensor and functional connectivity MRI analyses showing that connections between the temporoparietal junction and insula are asymmetrically lateralized to the right, while connections between the temporoparietal junction and the inferior frontal gyrus are asymmetrically lateralized to the left (Kucyi, Hodaie, & Davis, 2012).

It is also possible that the relationship between structural lateralization and functional lateralization is more than an artifact. Brain regions with more gray matter in one hemisphere may develop lateralization of brain functions ascribed to those regions.

Alternately, if a functional asymmetry develops in a brain region, it is possible that there may be hypertrophy of gray matter in that region. The extent to which structural and functional asymmetries co-evolve in development will require further study, including imaging at earlier points in development and with longitudinal imaging metrics, and whether asymmetric white matter projections (Iwabuchi et al., 2011; Kraemer, Yesavage, Taylor, & Kupfer, 2000) contribute to lateralization of functional connectivity.

It is important to note that our data measure only asymmetries in the magnitude of functional connectivity between homotopic connections, but do not measure differences in the content of cognitive information between analogous connections in opposite hemispheres. Thus, a connection in the left hemisphere could be associated with a completely novel neural computation from a homotopic connection in the right hemisphere yet show no difference in functional connectivity lateralization. Nevertheless, lateralized functional correlation suggests a network architecture that differs between the two hemispheres and may be an indicator of the content of the two networks given known differences in function of the respective left- and right-lateralized hubs.

We observed a weak generalized trend toward greater lateralization of connectivity with age between the 20 hubs included in the analysis, but most individual connections did not show significant age-related changes in lateralization. The weak changes in lateralization with age should be interpreted with caution because the correlations included >1000 data points, so very subtle differences may be observed that are not associated with behavioral or cognitive differences. Prior reports with smaller sample sizes have reported differences in lateralization during adolescence in prefrontal

cortex (Bergerbest et al., 2009) as well as decreased structural asymmetry with age over a similar age range (Kovalev, Kruggel, & von Cramon, 2003).

Similarly, we saw no differences in functional lateralization with gender. These results differ from prior studies in which significant gender differences in functional connectivity lateralization were reported (Liu et al., 2009; Tomasi & Volkow, 2012b). This may be due to differing methods between the two studies, including the use of short-range connectivity in one of the former reports and correction for structural asymmetries in this report. A prior study performing graph-theoretical analysis of resting state functional connectivity data using a predefined parcellation of the brain also found no significant effects of hemispheric asymmetry with gender, but reported that males tended to be more locally efficient in their right hemispheres and females tended to be more locally efficient in their left hemispheres (Tian, Wang, Yan, & He, 2011)

It is intriguing that two hubs of both the left-lateralized and right-lateralized network are nearly homotopic. Maximal left-lateralization in Broca area corresponds to a similar right-lateralized homotopic cluster extending to include the anterior insula in the salience network. Although both networks have bilateral homologues in the inferior frontal gyrus/anterior insular region, it is possible that the relative boundaries of Broca Homologue on the right and the frontoinsular salience region may "compete" for adjacent brain cortical function. Future studies in populations characterized for personality traits (Adelstein et al., 2011) or language function may be informative as to whether local connectivity differences in these regions are reflected in behavioral traits or abilities. The study is limited by the lack of behavioral data and subject ascertainment available in the subject sample. In particular, source data regarding handedness is lacking. However,

none of the hubs in our left- and right- lateralized networks involve primary motor or sensory cortices and none of the lateralized connections showed significant correlation with metrics of handedness in subjects for whom data were available.

Despite the need for further study of the relationship between behavior and lateralized connectivity, we demonstrate that left- and right-lateralized networks are homogeneously stronger among a constellation of hubs in the left and right hemispheres, but that such connections do not result in a subject-specific global brain lateralization difference that favors one network over the other (i.e., left-brained or right-brained). Rather, lateralized brain networks appear to show local correlation across subjects with only weak changes from childhood into early adulthood and very small if any differences with gender.

Table 3.1. Sources of open access datasets used for analysis of 1011 scans.

Site (FCON 1000)	*n* (Imaging Volumes)	Site (FCON 1000)	*n* (Imaging Volumes)	Site (ADD 200)	*n* (Imaging Volumes)
Ann Arbor	16 (295)	Leipzig	29 (195)	Kennedy Krieger	49 (124*)
Baltimore	11 (123)	New York	30 (192*)	NeuroImage	18 (261)
Bangor	1 (265)	Newark	15 (135)	NYU	87 (352*)
Beijing	187 (225)	Orangeburg	3 (165)	OHSU	22 (234)
Berlin	16 (195)	Oulu	33 (245)	Peking	109 (236)
Cambridge	171 (119)	Oxford	8 (175)	Pittsburgh	72 (196*)
Cleveland	5 (127)	Palo Alto	6 (175)	Washington U	35 (396*)
ICBM	13 (128)	Queensland	14 (190)		
Leiden	30 (215)	Saint Louis	31 (127)		

* Sites with multiple runs or sequences with differing numbers of imaging volumes. The reported number of imaging volumes is the most frequently used number per subject for the site.

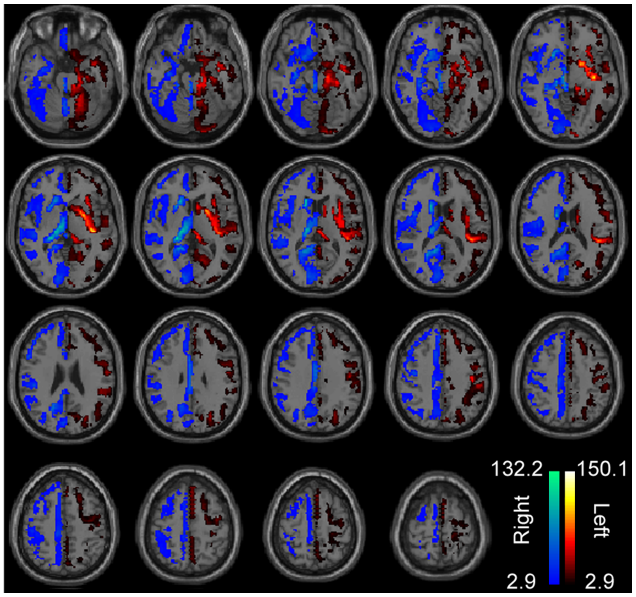

Figure 3.1: Significant lateralization of gray matter density. Colored regions included ROIs that showed significantly greater left- or right-lateralization of gray matter density across 1011 subjects, correcting for multiple comparisons using a false discovery rate correction of $q<0.05$ across 7266 ROIs. Color bars show *t*-statistics for the left and right hemispheres, respectively. Images are in radiologic format with subject left on image right.

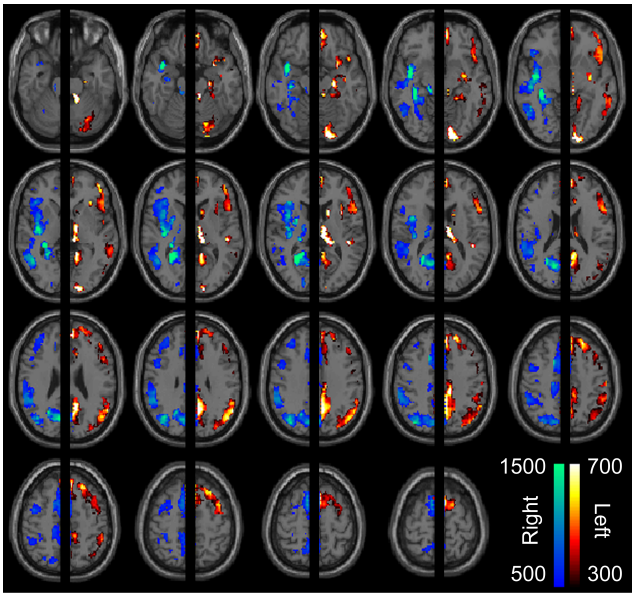

Figure 3.2. Degree maps for significantly left- and right-lateralized connections after regression of structural laterality index from all connections. Significantly lateralized connections (after correcting for multiple comparisons using a false discovery rate of $q < 0.05$, across all 14.1 million intrahemispheric connections) were used to construct a graph of significantly left-lateralized connections among left hemisphere ROIs and a separate graph of significantly right-lateralized connections among right hemisphere ROIs. Color scale shows graph-theoretical degree (i.e., sum of all significantly lateralized connections in which a given node is represented) for each ROI. Images are in radiologic format with subject left on image right.

Table 3.2. MNI coordinates of 20 lateralization hubs.

Left Hemisphere Hubs	X	Y	Z	Right Hemisphere Hubs	X	Y	Z
Broca Area (Br)	-45	25	0	Right Supplementary Motor Area (r-S)	5	8	61
Wernicke Area (We)	-58	-44	-2	Mid Insula (MI)	38	4	12
Inferior Dorsolateral Prefrontal Cortex (DP)	-43	43	1	Parietooccipital (PO)	36	-74	35
Left Supplementary Motor Area (l-S)	-6	10	62	Lateral Intraparietal Sulcus (LI)	55	-44	32
Lateral Premotor Cortex (LP)	-35	8	53	Frontal Eye Fields (FE)	43	0	51
Medial Prefrontal Cortex (MP)	-4	51	19	Dorsolateral Prefrontal Cortex (DL)	34	40	32
Medial Superior Frontal (SF)	-16	34	46	Middle Temporal Area (MT)	49	-60	0
Posterior Cingulate Cortex (PC)	-4	-56	31	Broca Homologue (Bh)	43	26	-3
Lateral Temporoparietal (TP)	-45	-67	30	Mid Cingulate Cortex (MC)	13	-32	47
				Superior Medial Intraparietal Sulcus (IP)	12	-73	44
				Anterior Insula (AI)	36	26	8

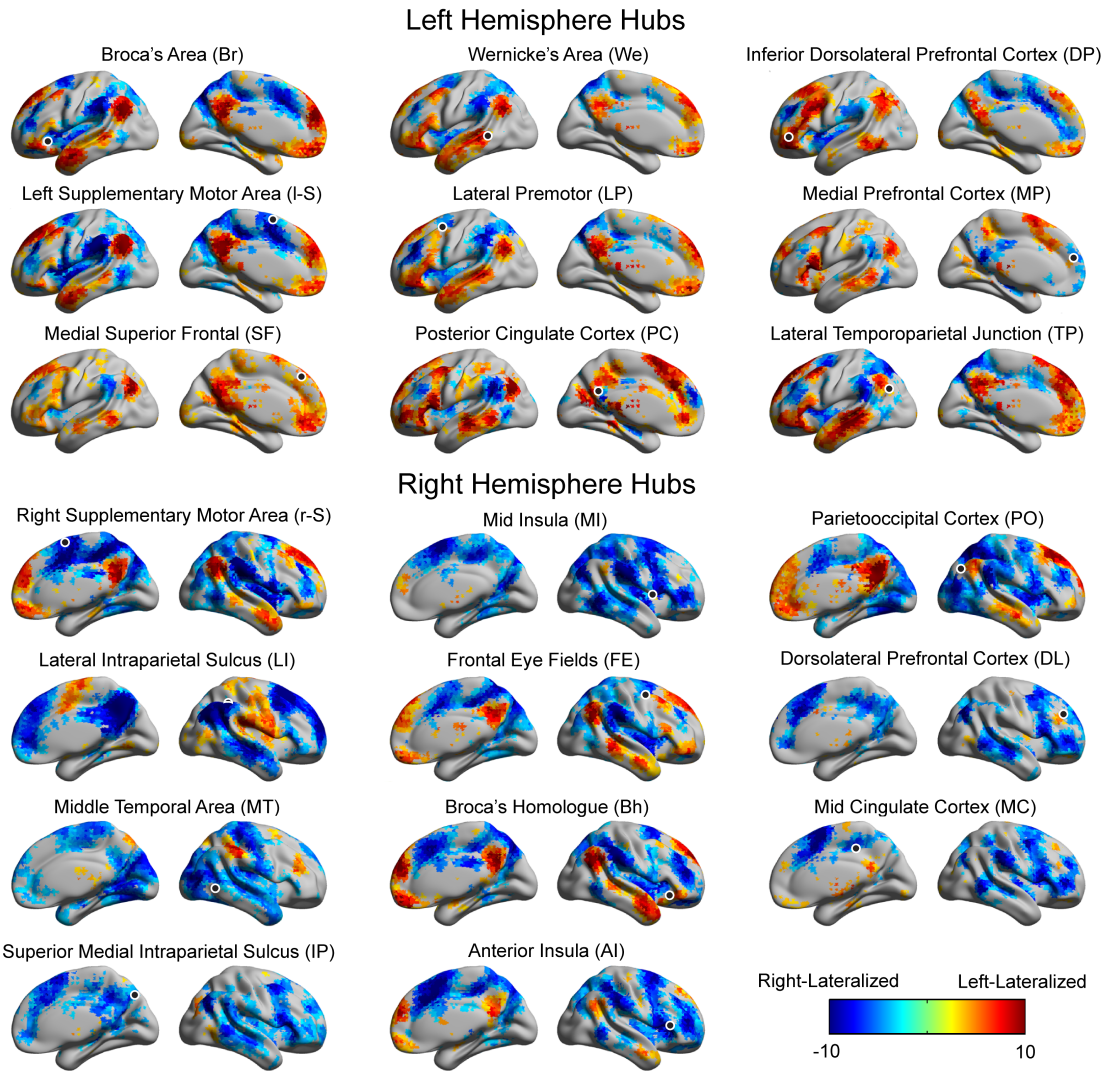

Figure 3.3. Significantly lateralized connections to each hub. The hemispheric lateralization maps for the 9 hubs of the left-lateralized network and 11 hubs of the right-lateralized network are shown in lateral and medial projections. Color scale (*t*-statistic) shows significantly left-lateralized (warm colors) or right-lateralized (cool colors) to the seed (i.e., hub). A black circle marks the position for each seed.

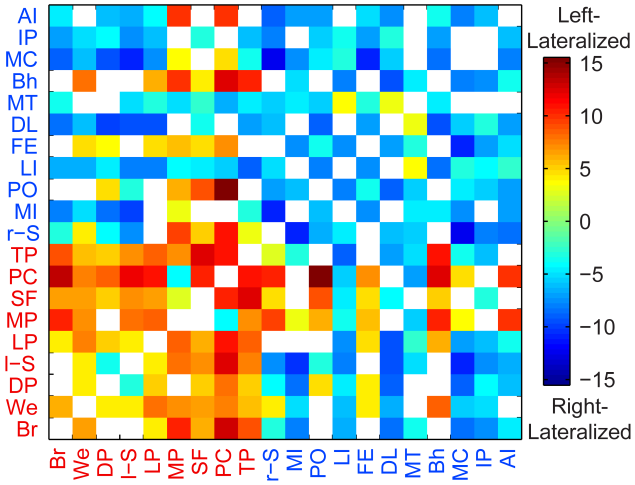

Figure 3.4: Significantly lateralized connections between each of the 20 hubs. Warm colors show significant left lateralization and cool colors show significant right lateralization. Color bar shows *t*-statistic for each connection. All colored squares were significant after correcting for multiple comparisons using a false discovery rate of $q<0.05$ among all possible connections between the hubs. See Table 3.2 or Figure 3.3 for the hubs' two-letter abbreviations.

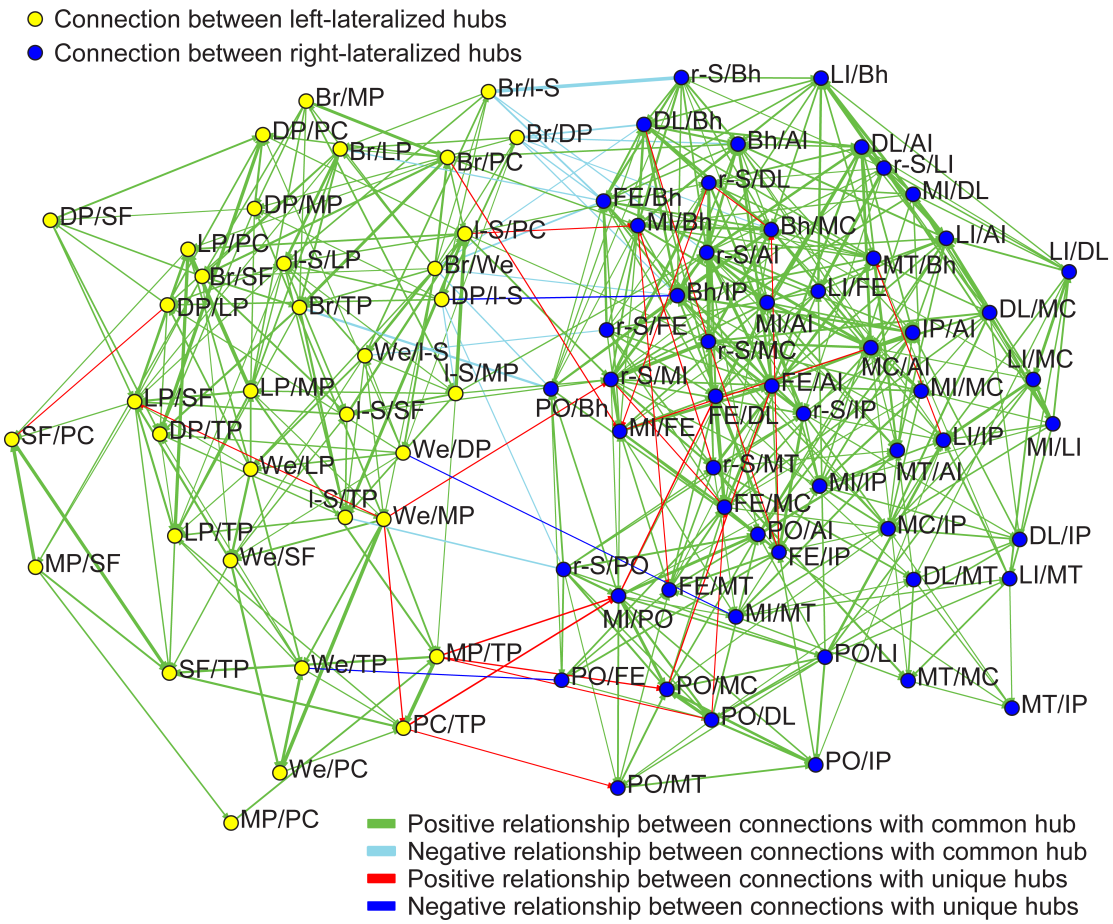

Figure 3.5. Significant correlation of lateralized connections across subjects. Yellow nodes represent connections between left hubs and green nodes represent connections between right hubs. An edge is present if lateralization was found to significantly correlate across subjects between the two connections, with red edges showing positive correlation and blue edges negative correlation, after correcting for multiple comparisons using a false discovery rate of $q<0.05$ across all possible connection-to-connection pairs. Virtually all edges are between nodes with a hub in common. A Kamada-Kawai algorithm was implemented in Social Network Image Animator software (http://www.stanford.edu/group/sonia/). The software was also used to visualize the relationship between connections. See Table 3.2 or Figure 3.3 for the hubs' two-letter abbreviations.

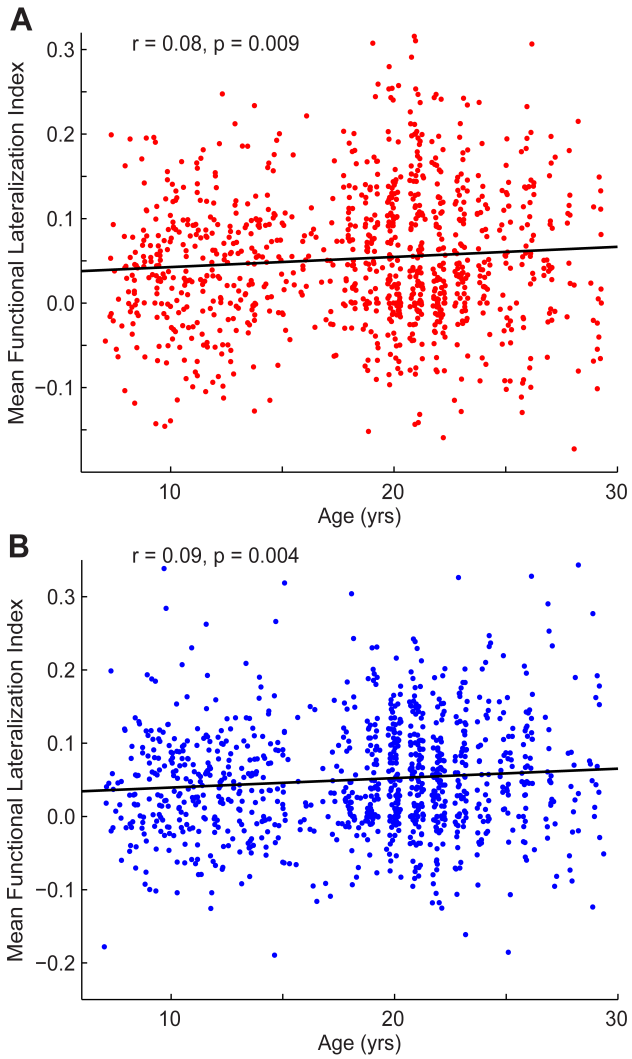

Figure 3.6. Change in mean functional lateralization with age. Mean functional lateralization index for all connections between left (A) and right (B) hubs, respectively, is shown for each subject, plotted against subject age. Pearson correlation coefficients and *p*-values are shown above both plots.

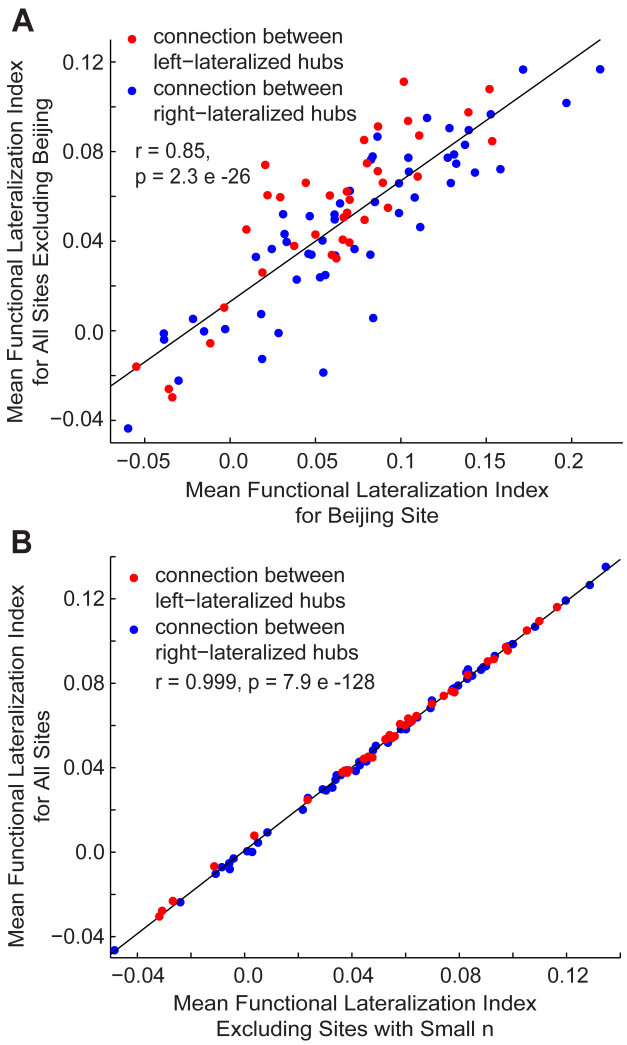

Figure 3.7. Reproducibility of lateralization. A) Mean functional lateralization index for the 91 intrahemispheric connections (blue, connections involving right-lateralized hubs; *red*, connections involving left-lateralized hubs) is compared when averaging across all subjects except those from the Beijing site and when averaging across only subjects from the Beijing site. Pearson correlation coefficients and *p*-values are shown in both plots. B) Mean functional lateralization index for the 91 intrahemispheric connections (*blue*, connections involving right-lateralized hubs; red, connections involving left-lateralized hubs) is compared when averaging across all subjects and when averaging across all subjects except those that come from a site with less than 10 subjects.

Table 3.3. Connections between right-lateralized hubs that change in lateralization across development between the ages of 7 and 29.

Hub 1	Hub 2	*r*	*p*
Right Supplementary Motor Area	Mid Insula	0.129	5.7e-5
Right Supplementary Motor Area	Middle Temporal Area	0.089	0.0052
Right Supplementary Motor Area	Mid Cingulate Cortex	0.084	0.0092
Mid Insula	Broca Homologue	0.116	0.0003
Parietooccipital	Frontal Eye Fields	0.099	0.0021
Parietooccipital	Mid Cingulate Cortex	0.110	0.0006
Lateral Intraparietal Sulcus	Broca Homologue	0.102	0.0013
Frontal Eye Fields	Middle Temporal Area	0.083	0.0087
Frontal Eye Fields	Mid Cingulate Cortex	0.088	0.0063
Frontal Eye Fields	Superior Medial Intraparietal Sulcus	0.128	6.9e-5

CHAPTER 4

LATERALIZATION OF FUNCTIONAL CONNECTIVITY IN AUTISM

Brain lateralization occurs during typical development (Toga & Thompson, 2003), and atypical lateralization in brain structure and function is associated with neuropsychiatric conditions and developmental disorders such as autism, schizophrenia, and specific language impairment (Chance et al., 2008; de Guibert et al., 2011; Fletcher et al., 2010; Herbert et al., 2002; Kleinhans, Muller, Cohen, & Courchesne, 2008; Lange et al., 2010b; Oertel-Knochel & Linden, 2011). More specifically, autism is associated with abnormal lateralization of brain function in core language regions, as measured by multiple functional imaging and electrophysiologic modalities.

Electroencephalographic studies have reported that evoked response lateralization during simple language stimuli in children with autism or high-risk infants was more often right-lateralized or lacked left lateralization compared to the typically developing children's left-lateralized evoked responses (Dawson, Finley, Phillips, & Galpert, 1986; Dawson, Finley, Phillips, & Lewy, 1989; Seery, Vogel-Farley, Tager-Flusberg, & Nelson, 2013). Also, lateralization of evoked response in children with autism correlated with language ability, where right lateralization related with poorer language ability (Dawson et al., 1986). Later studies utilizing positron emission tomography confirmed

that right lateralization exists in core language regions of adults (Boddaert et al., 2003; Muller et al., 1999) and children (Boddaert et al., 2004) with autism.

Functional magnetic resonance imaging (MRI) studies have found that typically developing individuals have significant left lateralization in language regions of the frontal lobe, whereas those with autism more commonly lack left lateralization or have reversed lateralization during language tasks (Kleinhans et al., 2008; Knaus, Silver, Lindgren, Hadjikhani, & Tager-Flusberg, 2008). Redcay et al. (2008) report a trend of left-lateralized function in typically developing toddlers listening to speech stimuli while sleeping (Redcay & Courchesne, 2008). Toddlers with autism show relative decrease in functional lateralization in Broca area or Wernicke area (Redcay & Courchesne, 2008). In a follow-up study to Redcay et al. (2008), Eyler et al. (2012) found that toddlers with autism have greater right-hemispheric activity in the temporal cortex in response to language (Eyler, Pierce, & Courchesne, 2012). This effect becomes more pronounced as the children with autism age (Eyler et al., 2012). Adolescents and adults with autism show decreased left-lateralized activity in response to language with greater bilaterality of functional activation (Anderson et al., 2010).

Studies of structural lateralization also report either a lack of left lateralization or a reversal in lateralization in autism. Herbert et al. (2002) parcellated the brain into 48 gyral regions per hemisphere and hypothesized that core language areas (i.e., Broca and Wernicke areas) would have abnormal volumetric lateralization in autism. Only gray matter volumes in Broca area were abnormally right-lateralized in autism participants (Herbert et al., 2002). In an exploratory whole-brain analysis, the authors also found that posterior temporal fusiform gyral volume was significantly more left-lateralized in autism

participants compared to typically developing participants (Herbert et al., 2002). Another volumetric lateralization analysis by the same group failed to find any group differences at the grossest parcellation level (i.e., total hemispheric volumes); however, as the parcellation scheme became finer in resolution, volumetric lateralization in autism was shifted to the right compared to typically developing individuals and a developmental language disorder group (Herbert et al., 2005). The majority of differences were due to either a loss of left lateralization or a gain of right lateralization in language (e.g., Broca area), face-processing (e.g., fusiform gyrus), and default mode (e.g., precuneus) regions (Herbert et al., 2005). De Fosse et al. (2004) found autism participants with language impairments and participants with specific language impairment had reversed volumetric laterality in Broca area, whereas typically developing participants and participants with autism but no language impairment had left-lateralized Broca area volumes (De Fosse et al., 2004). When lateralization of language function was investigated with a functional MRI task, autism had a greater proportion of atypical functional lateralization; however, functional lateralization rather than diagnosis accounted for a decrease in Broca area volumes and increase in white matter integrity in arcuate fasciculus (Knaus et al., 2010). In diffusion tensor imaging (DTI) studies, autism has decreased or reversed lateralization of white matter integrity in the arcuate fasciculus, superior temporal gyrus, cingulum, and uncinate fasciculus (Fletcher et al., 2010; Lange et al., 2010b; Lo et al., 2011).

Abnormal connectivity observations in autism have been made using both functional and structural connectivity analyses. These studies suggest the pathophysiology of autism includes widespread deficits across structural and functional networks, rather than deficits confined to a single brain region. In task-related functional

connectivity studies, those with autism had decreased connectivity in the motor execution network during a motor task (Mostofsky et al., 2009b), in the cortical language system during a sentence comprehension task (Just et al., 2004), in connections between the fusiform face area and other limbic structures during a face identification task (Kleinhans et al., 2008), and in connections between the parietal lobe and other brain regions during a working memory task (Koshino et al., 2005). The results of altered connectivity in the motor execution network and cortical language system are further supported by structural connectivity studies that employed DTI. The structural connectivity studies measured decreased fractional anisotropy, a measure of compromised white matter tract integrity, in the cerebellum (Catani et al., 2008; Cheng et al., 2010), the superior temporal gyrus (Lee et al., 2007), and the arcuate fasciculus (Fletcher et al., 2010) in autism.

In resting-state functional connectivity studies, autism is marked by decreased connectivity in the default mode network (Anderson et al., 2011d; Assaf et al., 2010; Kennedy & Courchesne, 2008a, 2008b; Kennedy et al., 2006; Monk et al., 2009; Weng et al., 2010), which is a set of spatially-distributed brain regions whose activity is associated with internal dialogue and narrative, autobiographical memory, mentalizing, and social processes (Buckner, Andrews-Hanna, & Schacter, 2008). Along with the default mode network, differences were found in the "social brain" (Gotts et al., 2012), which includes the regions of the default mode network among others, and in interhemispheric connections of homologous brain regions (Anderson et al., 2011). Increased connectivity has been seen for negatively correlated connections and for connections involving subcortical nuclei (Di Martino et al., 2010). These core findings have been confirmed in a multisite dataset with over 1000 subjects (Anderson et al., 2011; DiMartino et al., 2013).

These results from resting state analyses are confirmed in structural connectivity studies, again using DTI, that have found decreased fractional anisotropy in the default mode network and corpus callosum (Travers et al., 2012). Another recently employed technique, structural covariance MRI, investigates structural brain networks by correlating a group's gray matter measurement (e.g., cortical thickness, gray matter density, etc.) in one brain region with the gray matter measurement in other brain regions (Alexander-Bloch, Giedd, & Bullmore, 2013; Zielinski, Gennatas, Zhou, & Seeley, 2010). Children, adolescents, and young adults with autism have abnormal spatial distributions in structural covariance MRI networks that correspond to the default mode and salience networks (Zielinski et al., 2012).

As has been highlighted above, autism is characterized by abnormal lateralization of brain structure and function in regions specific to language. It is also more generally characterized by connectivity abnormalities across many large-scale brain networks. The first study to characterize whether functional lateralization abnormalities existed outside of language-specific regions found diffuse differences across many different functional networks (Cardinale, Shih, Fishman, Ford, & Muller, 2013). These widespread differences in functional lateralization existed in a small sample of children and adolescents, using independent component analysis to identify the functional networks.

Two recent reports describe how lateralized brain function segregates into two broad networks, a right- and left-lateralized network (Gotts et al., 2013a; Nielsen, Zielinski, Ferguson, Lainhart, & Anderson, 2013). The left-lateralized network appears to participate more in intrahemispheric connections, while the right-lateralized network participates in connections between hubs of the network and brain regions in both

hemispheres (Gotts et al., 2013a). In one report the broad networks include 20 lateralization hubs, 9 in the left-lateralized network and 11 in the right-lateralized network. The left-lateralized network includes core language regions (Broca area and Wernicke area) and regions of the default mode network (posterior cingulate cortex, medial prefrontal cortex, lateral temporal parietal junction, among other areas; (Nielsen et al., 2013). The right-lateralized network includes regions from three networks associated with attention to external stimuli: the dorsal and ventral attention networks and the frontoparietal executive network.

In the present study, we investigate these 20 lateralization hubs in autism and typical development and determine whether the lateralization of brain function differs between autism and typical development in a diffuse, network-wide manner or within isolated brain regions. We also determine whether lateralization of brain function correlates with clinical severity, age, and handedness.

Materials and Methods

Subject Sample

The Autism Brain Imaging Data Exchange (ABIDE) consists of 1112 datasets comprised of 539 autism and 573 typically developing individuals (DiMartino et al., 2013). Each dataset consists of one or more resting functional MRI acquisitions and a volumetric magnetization-prepared rapid acquisition with gradient echo (MPRAGE) image. All data are fully anonymized in accordance with HIPAA guidelines, with analyses performed in accordance with pre-approved procedures by the University of Utah Institutional Review Board. All images were obtained with informed consent

according to procedures established by human subjects research boards at each participating institution. Details of acquisition, informed consent, and site-specific protocols are available at http://fcon_1000.projects.nitrc.org/indi/abide/.

Inclusion criteria for subjects were successful preprocessing with manual visual inspection of normalization to Montreal Neurological Institute (MNI) space of MPRAGE, coregistration of blood-oxygen-level dependent (BOLD) and MPRAGE images, segmentation of MPRAGE image, and full brain coverage from MNI $z > -35$ to $z < 70$ on all BOLD images. Inclusion criteria for sites were a total of at least 20 subjects meeting all other inclusion criteria. A total of 964 subjects met all inclusion criteria (517 typically developing subjects and 447 subjects with autism from 16 sites and 19 datasets because 3 sites had multiple datasets). We also did secondary analyses using more strict inclusion criteria. The more strict inclusion criteria required, first, a subject have at least 50% of his or her resting state BOLD volumes remaining after motion scrubbing. Second, some of the ABIDE data for the typically developing controls were included in the 1000 Functional Connectomes (http://fcon_1000.projects.nitrc.org/) and/or ADHD-200 samples (http://fcon_1000.projects.nitrc.org/indi/adhd200/). The 1000 Functional Connectomes and ADHD-200 datasets were used as the basis for the 20 lateralization hubs interrogated in the present study (Nielsen et al., 2013). We were not able to determine which subjects were present in both the ABIDE sample and the 1000 Functional Connectomes or ADHD-200 samples due to anonymous submission of data to the publicly available samples. Therefore, we excluded sites where there was possible overlap in samples.

Each site followed different criteria for diagnosing patients with autism or ascertaining typical development, however, the majority of the sites used the Autism Diagnostic Observation Schedule (Lord et al., 2000) and Autism Diagnostic Interview-Revised (Lord et al., 1994). Specific diagnostic criteria for each site can be found at fcon_1000.projects.nitrc.org/indi/abide/index.html. Subject demographics for individuals satisfying inclusion criteria are shown in Table 4.1. Six different testing batteries were used to calculate verbal IQ and performance IQ, respectively. Specific IQ testing batteries and other behavioral measures for each site can be found at fcon_1000.projects.nitrc.org/indi/abide/index.html. In the case that no categorical measure (i.e., right-handed, left-handed, or ambidextrous) was reported, positive values were converted to right-handed, negative values to left-handed, and a value of zero to ambidextrous. Fifteen subjects lacked both a quantitative and categorical measurement of handedness.

BOLD Preprocessing

Preprocessing was performed in MATLAB (Mathworks, Natick, MA) using SPM8 (Wellcome Trust, London) software. The following sequence of preprocessing steps was performed:

1) Slice timing correction
2) Realign and reslice correction of motion for each volume relative to initial volume
3) Coregistration of BOLD images to MPRAGE anatomic sequence
4) Normalization of MPRAGE to MNI template brain, with normalization transformation also applied to coregistered BOLD images

5) Segmentation of gray matter, white matter (WM), and cerebrospinal fluid (CSF) components of MPRAGE image (thorough clean)
6) Extraction of mean time courses from the restriction masks applied to BOLD images from ROIs consisting of:
    a. CSF segmented mask with bounding box $-35 < x < 35$, $-60 < y < 30$, $0 < z < 30$
    b. White matter segmented mask overlapping with 10 mm radii spheres centered at x = -27, y = -7, z = 30, x = 27, y = -7, z = 30
    c. Mask of scalp and facial soft tissues (Anderson et al., 2011a)
7) Voxelwise bandpass filter (0.001 to 0.1 Hz) and linear detrend, performed concurrently with step 8.
8) Voxelwise regression using glmfit.m (MATLAB Statistics Toolbox) software of CSF, WM, Soft tissue, and 6 motion parameters from realignment step from time series of each voxel of BOLD images
9) Motion scrubbing (Power et al., 2012) of framewise displacement and DVARS with removal of volumes before and after a root-mean-square displacement of > 0.2 for either parameter and concatenation of remaining volumes
10) No spatial smoothing was performed to avoid contaminating the signal near the midsagittal plane. The global mean signal and gray matter time courses were not regressed from voxelwise data (Anderson et al., 2011a; Gotts et al., 2013b; Murphy et al., 2009; Saad et al., 2012).

ROI Analysis

From preprocessed BOLD images for each subject, mean time course was extracted from 7266 gray matter ROIs. These ROIs from a lattice covering the grey.nii image (SPM8) from z = -35 to z = 70 at 5-mm resolution, with MNI coordinates of centroids previously reported (Anderson et al., 2011d). The ROIs averaged 4.9 +/- 1.3 standard deviation voxels in size for 3 mm isotropic voxels. A 7266 x 7266 matrix of Fisher-transformed Pearson correlation coefficients was obtained for each subject from the ROI timecourses representing an association matrix of functional connectivity in each subject between all pairs of ROIs. Each pair of ROIs is termed a "connection" for the present analysis.

Functional Lateralization Metric

Functional correlation was obtained as the Fisher-transformed Pearson correlation coefficient between each pair of the 7266 ROIs within the same hemisphere. We only analyzed connections within a single hemisphere and the opposite hemisphere homologues because of ambiguity of "lateralization" of a cross-hemisphere connection. Preprocessed images were inverted across the midsagittal plane, and analogous Fisher-transformed correlation coefficients were obtained between each pair of the same ROIs on the flipped images. Functional lateralization index was defined as the difference (unflipped - flipped) between Fisher-transformed correlation coefficients.

In a previous study of typical development, 20 cortical regions were identified as lateralization hubs, or brain regions involved in the most functionally-lateralized connections (Figure 4.1; (Nielsen et al., 2013). The 20 lateralization hubs were a subset

of 7,266 ROIs described above and comprised 9 left-hemispheric regions and 11 right-hemispheric regions. All analyses in the present study focused on connections between the 20 lateralization hubs. For the MNI coordinates of the 20 lateralization hubs and more information on the methods for identifying the lateralization hubs, refer to Nielsen et al. (2013).

Statistical Analyses

All statistical analyses were performed in MATLAB using MATLAB's statistical toolbox. Each lateralization hub's pattern of lateralization with other hubs in the ipsilateral hemisphere of the cerebral cortex was determined separately for the typically developing group and the autism group by performing one-sample *t*-tests on the functional connections involving the cortical hub as the seed and the other ipsilateral hubs (Figure 4.2). We corrected for multiple comparisons using a false discovery rate of $q < 0.05$.To test for group differences in lateralization of intrinsic connectivity, two-sample *t*-tests were applied on the set of ipsilateral connections involving the 20 lateralization hubs (36 left-lateralized connections and 55 right-lateralized connections; Figures 4.1 and 4.2). We again corrected for multiple comparisons using a false discovery rate of $q < 0.05$. We also used different inclusion criteria for the subjects when testing group differences in lateralization of the 91 lateralized connections (Table 4.2). To test for the effect of clinical severity, age, and handedness, Pearson correlation coefficients were calculated across all participants for the three connections with abnormal lateralization when comparing the typically developing group to the autism group (Figure 4.3).

Results

We investigated the lateralization patterns among the lateralization hubs of the left- and right-lateralized networks in typical development and autism, and then compared the lateralization patterns of the two groups. In the typically developing group, strong lateralization existed between the hubs of the left- and right-lateralized networks, respectively (Figure 4.2A). In the autism group, lateralization between the hubs also existed, although not as strongly as in the typically developing group (Figure 4.2B). When comparing the two groups, the majority of the differences existed in connections involving specific left-lateralized hubs (Figure 4.1 and Figure 4.2C). Only three of the connections survived multiple comparisons correction using a false discovery rate of $q < 0.05$. The three connections were in the left-lateralized network—Wernicke area to the posterior cingulate cortex; Wernicke area to the temporoparietal junction; and Broca area to the posterior cingulate cortex. All three either lacked left lateralization or had greatly diminished left lateralization in the autism group compared to the typically developing group (Wernicke-posterior cingulate: $t(961) = 3.36$, $p = 0.0008$; Wernicke-temporoparietal: $t(962) = 3.30$, $p= 0.001$; Broca-posterior cingulate: $t(960) = 3.04$, $p = 0.002$).

We also repeated the analyses that identified the group differences in lateralized functional connections, using three additional inclusion criteria to determine which subjects would be included in the analysis (Table 4.2). Regardless of which inclusion criteria was used for the subjects, the connection involving Wernicke area and posterior cingulate cortex and the connection involving Wernicke area and temporoparietal junction were abnormal in the autism group. Four other connections were abnormal in at

least one of the four inclusion criteria analyses, all involving core language regions and default mode regions in the left-lateralized network.

Finally, we investigated the relationship between lateralization in the three abnormal connections and autism severity, age, and handedness. The connection between Wernicke area and the posterior cingulate cortex negatively correlated with autism severity ($r(346) = -0.13$, $p = 0.02$; Figure 4.3). As left lateralization decreased between Wernicke area and posterior cingulate cortex, autism severity increased. No significant relationships between lateralization and age or lateralization and handedness were found.

Discussion

In this study, we tested brain lateralization in autism using functional connectivity MRI and found that abnormal lateralization of functional connectivity during rest in autism is restricted to specific left-lateralized connections that involve language regions (i.e., Broca area and Wernicke area) and regions of the default mode network (i.e., temporoparietal junction and posterior cingulate cortex), rather than diffusely affecting either the left- or right-lateralized functional networks. We also replicated previous results in the typically developing group that two interconnected lateralized networks exist in the brain, one in the left hemisphere, and one in the right hemisphere, with the left-lateralized network involving language and default mode regions, and the right-lateralized network involving brain attentional regions (Nielsen et al., 2013).

Cardinale and colleagues found that abnormal lateralization in autism existed across many intrinsic networks, including primary sensory and higher-level association networks (Cardinale et al., 2013). We, too, found either a lack of left lateralization or

greater right lateralization in the autism group; however, the regions or networks involved in abnormal lateralization differed. Rather than finding abnormalities throughout a number of networks as Cardinale and colleagues did, we only found differences in a handful of connections involving language regions and regions of the default mode network. Cardinale and colleagues did find lateralization in the default mode network in some of their supplemental analyses; however, they did not directly test lateralization between language regions and default mode regions. The inconsistent results are most likely due to differences in the sample age, sample size, number of data acquisition sites, and/or data analysis methods.

We also found that abnormal lateralization relates to clinical severity, which corresponds with previous reports of abnormal brain lateralization and intrinsic connectivity in general. In individuals with autism, reduced functional connectivity within the default mode network relates to more social and communication impairments (Anderson et al., 2011d; Assaf et al., 2010; Gotts et al., 2012; Monk et al., 2009; Weng et al., 2010). Cardinale and colleagues did not find a relationship between abnormal lateralization of intrinsic networks and social or communication impairments that survived multiple comparisons (Cardinale et al., 2013).

The abnormal lateralization of connections involving regions of the default mode network and core language regions may represent an overall lack of specialization in brain regions that process language and social stimuli. Regions of the default mode network are involved in tasks that require language (e.g., internal narrative and autobiographical memory) and theory of mind or understanding of another's mental state (Buckner et al., 2008; Gusnard et al., 2001; Saxe & Kanwisher, 2003). The

temporoparietal junction and posterior cingulate cortex participate in the same component as core language regions during a language task (Geranmayeh et al., 2012). The temporoparietal junction participates in both semantic tasks and deactivates during cognitively taxing tasks (i.e., has default mode characteristics; (Seghier, Fagan, & Price, 2010). The posterior cingulate cortex is more active in congruent and coherent language compared to incongruent or incoherent language (Ferstl, Neumann, Bogler, & von Cramon, 2008; Tesink et al., 2009b). The right inferior frontal gyrus is more active in autism compared to typical development during a language task, implying abnormal lateralization in a core language region that may have implications in its relationship with other brain regions (e.g., as we found with the connection between Broca area and posterior cingulate cortex; (Tesink et al., 2009a). Together these observations suggest the abnormal lateralization between core language regions and default mode regions could account for some of the communication and social deficits experienced by individuals with autism. This possibility is also supported by findings that abnormal lateralization in language regions are correlated with decreased function on standardized testing (Gotts et al., 2013a).

The observation that abnormal functional lateralization in autism is limited to connections between core language regions constrains hypotheses of developmental pathophysiology in autism. Our analysis suggests that abnormal language lateralization in autism may be due to abnormal language development rather than a deficit in hemispheric specialization of the entire brain, and would be more consistent with a search for mechanisms involving brain substrates for language acquisition rather than earlier potential mechanisms where hemispheric asymmetries emerge. This constraint is also

supported by multimodal observations from DTI, functional MRI, structural MRI, and electrophysiologic studies that have all identified specific deficits in language-related lateralization but not differences in lateralization in other cognitive subsystems.

While the large sample size of the ABIDE dataset can be a tremendous advantage for improving statistical power and external generalizability of the results, it can also be a liability. The individual sites differ in many important data acquisition variables including inclusion criteria, demographics, pulse sequence, scanner type, and length of scan. Most of the included scans were very short, less than 10 minutes duration per subject. It is possible that the heterogeneity of the dataset may limit sensitivity for detecting small changes, and that in a more homogenous data sample additional differences in lateralization would be found.

An additional limitation is that we did not attempt a discovery of all lateralization differences in an attempt to control the multiple comparison problem that would arise, but instead looked for lateralization differences only between a set of 20 regions that were previously identified as being hubs of lateralized networks in a control population (different from the control subjects used here). It is possible that systematic differences in lateralization are present in brain regions that are not necessarily hubs of lateralization networks in the brain, and which we could not detect.

In conclusion, brain lateralization occurs in typical development and is abnormal in autism. As has been shown in multiple reports, left lateralization of core language regions in autism is diminished. In addition to core language regions, we have shown that the synchronization between core language regions and default mode regions lacks left-sided lateralization in autism. The abnormal lateralization correlates with more severe

communication and social deficits. These abnormalities represent differences that persist from childhood throughout adulthood, in at least a subgroup of individuals with autism, and suggest a lack of specialization.

Table 4.1. Subjects included from the ABIDE sample with demographic information.

	Age	ADOS-G total	Handedness (left, right, ambidextrous)	Handedness (-100 – +100)	Verbal IQ	Performance IQ
Number of subjects	964	348	949	348	781	796
Control	(426 M, 91 F)	32	(472 R, 34 L, 3 A)	184	413	425
Autism	(396 M, 51 F)	316	(378 R, 58 L, 4 A)	164	367	371
Control mean +/- s.d.	16.9 +/- 7.56	1.25 +/- 1.37	N/A	67.4 +/- 39.0	112 +/- 13.3	108 +/- 13.3
(Control range)	(6.47 - 56.2)	(0 - 4)	N/A	(-100 – +100)	(67 - 147)	(67 - 155)
Autism mean +/- s.d.	16.6 +/- 8.1	11.9 +/- 3.81	N/A	51.8 +/- 54.5	105 +/- 17.4	106 +/- 17.2
(Autism range)	(7 - 64)	(2 - 22)	N/A	(-100 – +100)	(50 - 149)	(59 - 157)

Table 4.2. Group differences in lateralization for various subject inclusion criteria.

Inclusion criteria	Total *n* (Autism *n*)	ROI 1	ROI 2	*t*	*p*
A	964 (447)	Posterior cingulate	Wernicke	3.37	7.7×10^{-4}
		Posterior cingulate	Broca	3.04	2.4×10^{-3}
		Temporoparietal junction	Wernicke	3.63	2.9×10^{-4}
B	831 (362)	Posterior cingulate	Wernicke	3.39	7.2×10^{-4}
		Posterior cingulate	Lateral premotor	2.93	3.5×10^{-3}
		Temporoparietal junction	Wernicke	3.66	2.7×10^{-4}
C	765 (447)	Posterior cingulate	Wernicke	3.69	2.4×10^{-4}
		Posterior cingulate	Broca	3.52	4.6×10^{-4}
		Posterior cingulate	Lateral premotor	3.63	3.0×10^{-4}
		Posterior cingulate	Left supplementary motor area	2.74	6.3×10^{-3}
		Temporoparietal junction	Wernicke	3.78	1.6×10^{-4}
		Temporoparietal junction	Left supplementary motor area	2.87	4.2×10^{-3}
D	645 (362)	Posterior cingulate	Wernicke	3.83	1.4×10^{-4}
		Posterior cingulate	Lateral premotor	3.79	1.7×10^{-4}
		Temporoparietal junction	Wernicke	3.71	2.3×10^{-4}

A: Met all preprocessing criteria (described in Methods and Materials section) and part of site with >20 subjects
B: Criteria A + subject has >50% resting state BOLD volumes after motion scrubbing
C: Criteria A + subject not included in 1000 Functional Connectomes or ADHD200 datasets
D: Criteria A + B + C

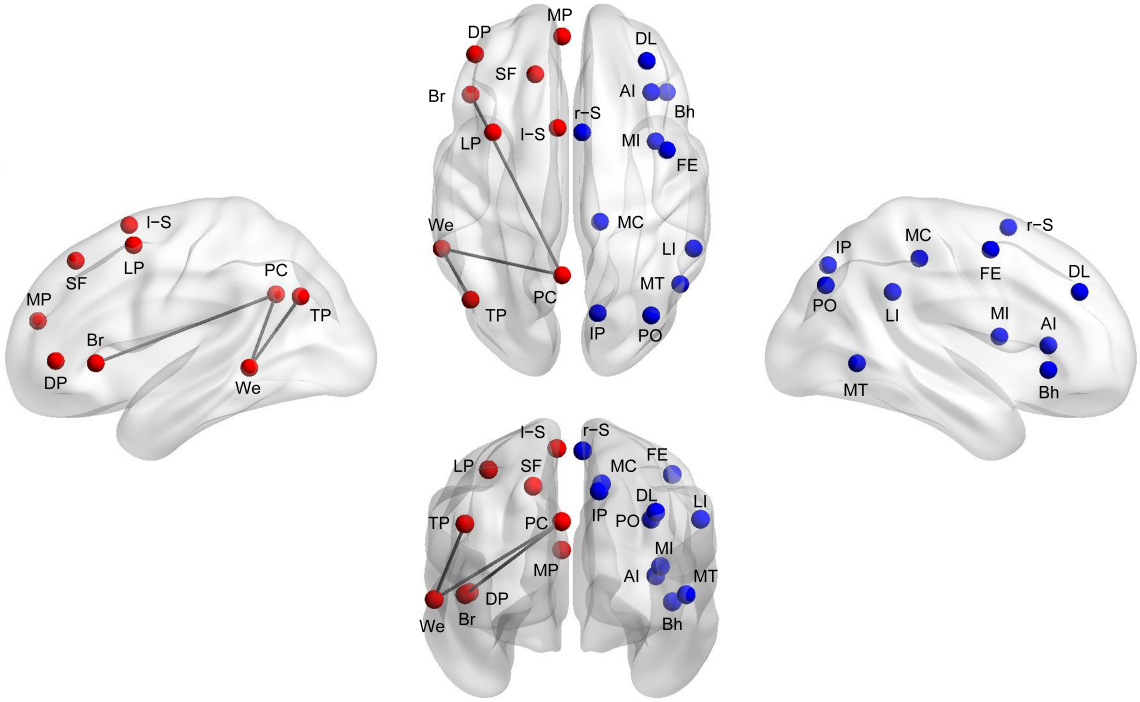

Figure 4.1. Lateralized hub locations and abnormally lateralized connections. The left- (*red*) and right-lateralized (*blue*) brain regions that participate in the most left- and right-lateralized connections, as determined in a separate sample of 1011 typically developing subjects, are displayed on rendered brain images. Three connections (*black lines*) are less left-lateralized in the autism group compared to the typically developing group when all 964 subjects are included in the analysis. Abbreviations: Broca area (Br), Wernicke area (We), inferior dorsolateral prefrontal cortex (DP), left supplementary motor area (l-S), lateral premotor cortex (LP), medial prefrontal cortex (MP), medial superior frontal cortex (SF), posterior cingulate cortex (PC), temporoparietal junction (TP), right supplementary motor area (r-S), mid insula (MI), parietooccipital cortex (PO), lateral intraparietal sulcus (LI), frontal eye fields (FE), dorsolateral prefrontal cortex (DL), middle temporal area (MT), Broca homologue (Bh), mid cingulate cortex (MC), superior medial intraparietal sulcus (IP), anterior insula (AI).

Figure 4.2. Group lateralization patterns. The lateralization patterns of the connections involving the 20 lateralized hubs displayed in the typically developing group (A), autism group (B), and group differences (C). The colored connections (i.e., squares of the plot) represent a group difference of $p < 0.05$ and colored connections with asterisk represent a group difference that survives multiple comparisons correction using a false discovery rate of $q < 0.05$. See Figure 4.1's legend for list of abbreviations.

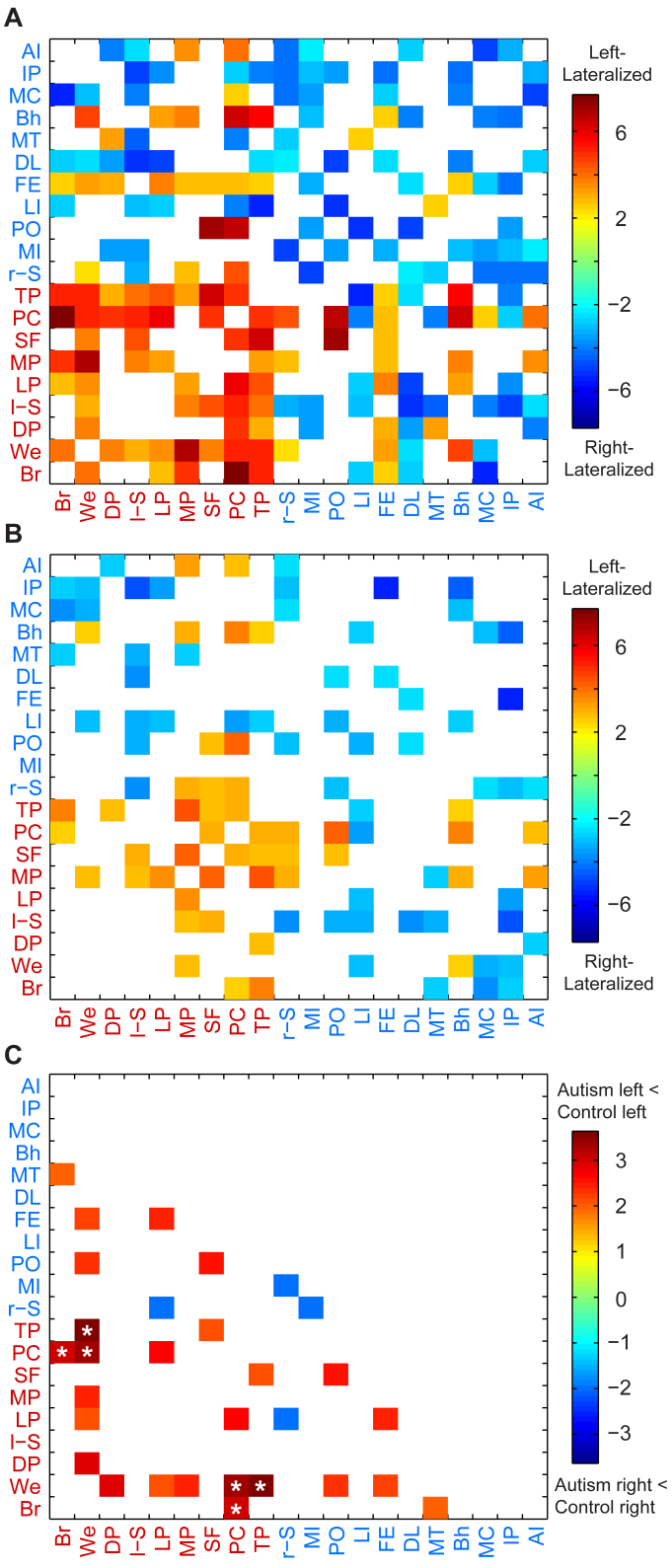
A
AI
IP
MC
Bh
MT
DL
FE
LI
PO
MI
r−S
TP
PC
SF
MP
LP
I−S
DP
We
Br
Left-
Lateralized
6
2
−2
−6
Right-
Lateralized
B
C
Autism left <
Control left
3
2
1
0
−1
−2
−3
Autism right <
Control right

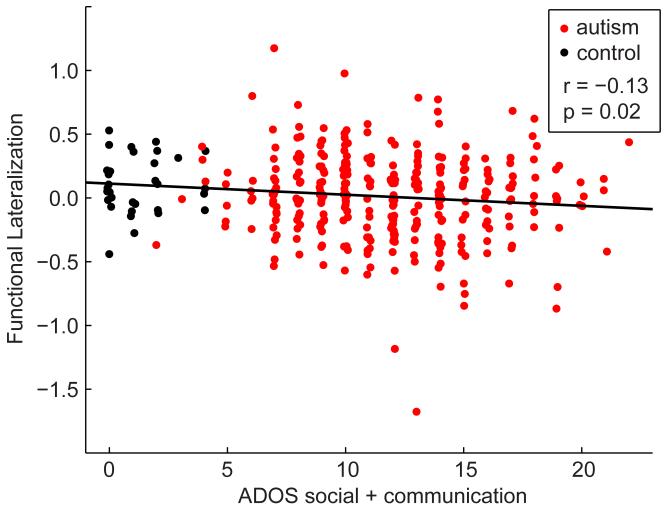

Figure 4.3. Relationship between lateralization and autism severity. The left lateralization of the functional connection involving Wernicke area and posterior cingulate cortex shares a negative correlation with autism severity, as calculated by adding the ADOS-G social and communication domains' total scores for each subject with autism (*red*) and typically developing subject (*black*) separately. See plot for correlation coefficient and corresponding *p*-value.

CHAPTER 5

CONCLUSIONS

The first conclusion of these studies is that much work must still be done to develop technologies and methods that will allow for across site classification algorithms to be implemented. The signal-to-noise ratio when comparing the biological signal introduced by individuals with autism to the noise introduced by different scanners and parameters used in MR imaging is low. One point to consider going forward is the length of time an individual is scanned. The synchrony in brain activity between two different regions is fairly stable after 5 minutes of scanning (Van Dijk et al., 2010); however, in order to use functional connectivity analyses to distinguish a single person from a group, longer imaging time must be used (Anderson et al., 2011).

The second conclusion is that, contrary to popular belief among the lay public, individuals are not “left brained” or “right-brained.” We showed that the brain is made up of two lateralized networks, a right-lateralized network made up of attentional regions and a left-lateralized network made up of core language regions and default mode regions. We also showed that if the synchrony between two regions in the left-lateralized network is strongly synchronous, it has no bearing on how synchronous the other connections are in the left- or right-lateralized networks.

Finally, the third conclusion is that individuals with autism lack left lateralization in connections involving core language regions and default mode regions. These abnormalities relate to disorder severity, and may underlie the communication and language deficits. They may also reflect an abnormal interface between language regions involved internal dialogue (e.g., default mode regions) and regions involved in processing speech and producing speech (e.g., Broca and Wernicke areas).

REFERENCES

Achard, S., Salvador, R., Whitcher, B., Suckling, J., & Bullmore, E. (2006). A resilient, low-frequency, small-world human brain functional network with highly connected association cortical hubs. *J Neurosci, 26*(1), 63-72.

Adelstein, J. S., Shehzad, Z., Mennes, M., Deyoung, C. G., Zuo, X. N., Kelly, C., Margulies, D. S., Bloomfield, A., Gray, J. R., Castellanos, F. X., & Milham, M. P. (2011). Personality is reflected in the brain's intrinsic functional architecture. *PLoS One, 6*(11), e27633.

ADHD-200_Consortium. (2012). The adhd-200 consortium: A model to advance the translational potential of neuroimaging in clinical neuroscience. *Front Syst Neurosci, 6*, 62.

Alexander-Bloch, A., Giedd, J. N., & Bullmore, E. (2013). Imaging structural co-variance between human brain regions. *Nat Rev Neurosci, 14*(5), 322-336.

Anderson, J. S. (2013). Functional connectivity MRI in autism. *Imaging the brain in autism* (pp. 325-347): Springer New York.

Anderson, J. S., Dhatt, H. S., Ferguson, M. A., Lopez-Larson, M., Schrock, L., House, P., & Yurgelun-Todd, D. (2011). Functional connectivity targeting for deep brain stimulation in essential tremor. *AJNR Am J Neuroradiol, 32*, 1963-1968.

Anderson, J. S., Druzgal, T. J., Froehlich, A., Dubray, M. B., Lange, N., Alexander, A. L., Abildskov, T., Nielsen, J. A., Cariello, A. N., Cooperrider, J. R., Bigler, E. D., & Lainhart, J. E. (2011). Decreased interhemispheric functional connectivity in autism. *Cereb Cortex, 21*(5), 1134-1146.

Anderson, J. S., Druzgal, T. J., Lopez-Larson, M., Jeong, E. K., Desai, K., & Yurgelun-Todd, D. (2011a). Network anticorrelations, global regression, and phase-shifted soft tissue correction. *Hum Brain Mapp, 32*(6), 919-934.

Anderson, J. S., Ferguson, M. A., Lopez-Larson, M., & Yurgelun-Todd, D. (2011). Connectivity gradients between the default mode and attention control networks. *Brain Connectivity, 1*(2), 147-157.

Anderson, J. S., Ferguson, M. A., Lopez-Larson, M., & Yurgelun-Todd, D. (2011b). Reproducibility of functional connectivity measurements in single subjects. *AJNR Am J Neuroradiol, 32*, 548-555.

Anderson, J. S., Ferguson, M. A., Lopez-Larson, M., & Yurgelun-Todd, D. (2011). Reproducibility of single-subject functional connectivity measurements. *AJNR Am J Neuroradiol*.

Anderson, J. S., Ferguson, M. A., Lopez-Larson, M., & Yurgelun-Todd, D. (2011c). Reproducibility of single-subject functional connectivity measurements. *AJNR Am J Neuroradiol, 32*(3), 548-555.

Anderson, J. S., Ferguson, M. A., & Nielsen, J. A. (2013a). Functional MRI in autism. *Imaging the brain in autism* (pp. 289-323): Springer New York.

Anderson, J. S., Lange, N., Froehlich, A., DuBray, M., Druzgal, T., Froimowitz, M., Alexander, A., Bigler, E., & Lainhart, J. (2010). Decreased left posterior insular activity during auditory langauge in autism. *AJNR Am J Neuroradiol, 31*, 131-139.

Anderson, J. S., Nielsen, J. A., Ferguson, M. A., Burback, M. C., Cox, E. T., Dai, L., Gerig, G., Edgin, J. O., & Korenberg, J. R. (2013b). Abnormal brain synchrony in down syndrome. *NeuroImage: Clinical, 2*, 703-715.

Anderson, J. S., Nielsen, J. A., Froehlich, A. L., DuBray, M. B., Druzgal, T. J., Cariello, A. N., Cooperrider, J. R., Zielinski, B. A., Ravichandran, C., & Fletcher, P. T. (2011d). Functional connectivity magnetic resonance imaging classification of autism. *Brain, 134*(12), 3739-3751.

Anderson, J. S., Zielinski, B. A., Nielsen, J. A., & Ferguson, M. A. (2013c). Complexity of low‐frequency blood oxygen level‐dependent fluctuations covaries with local connectivity. *Human brain mapping*.

Andrews-Hanna, J. R., Reidler, J. S., Huang, C., & Buckner, R. L. (2010). Evidence for the default network's role in spontaneous cognition. *J Neurophysiol, 104*(1), 322-335.

Andrews-Hanna, J. R., Reidler, J. S., Sepulcre, J., Poulin, R., & Buckner, R. L. (2010). Functional-anatomic fractionation of the brain's default network. *Neuron, 65*(4), 550-562.

Assaf, M., Jagannathan, K., Calhoun, V. D., Miller, L., Stevens, M. C., Sahl, R., O'Boyle, J. G., Schultz, R. T., & Pearlson, G. D. (2010). Abnormal functional connectivity

of default mode sub-networks in autism spectrum disorder patients. *Neuroimage, 53*(1), 247-256.

Bergerbest, D., Gabrieli, J. D., Whitfield-Gabrieli, S., Kim, H., Stebbins, G. T., Bennett, D. A., & Fleischman, D. A. (2009). Age-associated reduction of asymmetry in prefrontal function and preservation of conceptual repetition priming. *Neuroimage, 45*(1), 237-246.

Biswal, B. B., Mennes, M., Zuo, X. N., Gohel, S., Kelly, C., Smith, S. M., Beckmann, C. F., Adelstein, J. S., Buckner, R. L., Colcombe, S., Dogonowski, A. M., Ernst, M., Fair, D., Hampson, M., Hoptman, M. J., Hyde, J. S., Kiviniemi, V. J., Kotter, R., Li, S. J., Lin, C. P., Lowe, M. J., Mackay, C., Madden, D. J., Madsen, K. H., Margulies, D. S., Mayberg, H. S., McMahon, K., Monk, C. S., Mostofsky, S. H., Nagel, B. J., Pekar, J. J., Peltier, S. J., Petersen, S. E., Riedl, V., Rombouts, S. A., Rypma, B., Schlaggar, B. L., Schmidt, S., Seidler, R. D., Siegle, G. J., Sorg, C., Teng, G. J., Veijola, J., Villringer, A., Walter, M., Wang, L., Weng, X. C., Whitfield-Gabrieli, S., Williamson, P., Windischberger, C., Zang, Y. F., Zhang, H. Y., Castellanos, F. X., & Milham, M. P. (2010). Toward discovery science of human brain function. *Proc Natl Acad Sci U S A, 107*(10), 4734-4739.

Boddaert, N., Belin, P., Chabane, N., Poline, J. B., Barthelemy, C., Mouren-Simeoni, M. C., Brunelle, F., Samson, Y., & Zilbovicius, M. (2003). Perception of complex sounds: Abnormal pattern of cortical activation in autism. *Am J Psychiatry, 160*(11), 2057-2060.

Boddaert, N., Chabane, N., Belin, P., Bourgeois, M., Royer, V., Barthelemy, C., Mouren-Simeoni, M. C., Philippe, A., Brunelle, F., Samson, Y., & Zilbovicius, M. (2004). Perception of complex sounds in autism: Abnormal auditory cortical processing in children. *Am J Psychiatry, 161*(11), 2117-2120.

Buckner, R. L., Andrews-Hanna, J. R., & Schacter, D. L. (2008). The brain's default network: Anatomy, function, and relevance to disease. *Ann N Y Acad Sci, 1124*, 1-38.

Buckner, R. L., Sepulcre, J., Talukdar, T., Krienen, F. M., Liu, H., Hedden, T., Andrews-Hanna, J. R., Sperling, R. A., & Johnson, K. A. (2009). Cortical hubs revealed by intrinsic functional connectivity: Mapping, assessment of stability, and relation to alzheimer's disease. *J Neurosci, 29*(6), 1860-1873.

Calderoni, S., Retico, A., Biagi, L., Tancredi, R., Muratori, F., & Tosetti, M. (2012). Female children with autism spectrum disorder: An insight from mass-univariate and pattern classification analyses. *NeuroImage, 59*(2), 1013-1022.

Cardinale, R. C., Shih, P., Fishman, I., Ford, L. M., & Muller, R. A. (2013). Pervasive rightward asymmetry shifts of functional networks in autism spectrum disorder. *JAMA Psychiatry, In press*.

Catani, M., Jones, D. K., Daly, E., Embiricos, N., Deeley, Q., Pugliese, L., Curran, S., Robertson, D., & Murphy, D. G. (2008). Altered cerebellar feedback projections in asperger syndrome. *Neuroimage, 41*(4), 1184-1191.

Cavanna, A. E., & Trimble, M. R. (2006). The precuneus: A review of its functional anatomy and behavioural correlates. *Brain, 129*(Pt 3), 564-583.

Chance, S. A., Casanova, M. F., Switala, A. E., & Crow, T. J. (2008). Auditory cortex asymmetry, altered minicolumn spacing and absence of ageing effects in schizophrenia. *Brain, 131*(Pt 12), 3178-3192.

Cheng, Y., Chou, K. H., Chen, I. Y., Fan, Y. T., Decety, J., & Lin, C. P. (2010). Atypical development of white matter microstructure in adolescents with autism spectrum disorders. *Neuroimage, 50*(3), 873-882.

Cherkassky, V. L., Kana, R. K., Keller, T. A., & Just, M. A. (2006). Functional connectivity in a baseline resting-state network in autism. *Neuroreport, 17*(16), 1687-1690.

Constantino, J. N., & Todd, R. D. (2003). Autistic traits in the general population: A twin study. *Arch Gen Psychiatry, 60*(5), 524-530.

Corbetta, M., & Shulman, G. L. (2002). Control of goal-directed and stimulus-driven attention in the brain. *Nat Rev Neurosci, 3*(3), 201-215.

Corbetta, M., & Shulman, G. L. (2011). Spatial neglect and attention networks. *Annu Rev Neurosci, 34*, 569-599.

Coutanche, M. N., Thompson-Schill, S. L., & Schultz, R. T. (2011). Multi-voxel pattern analysis of fMRI data predicts clinical symptom severity. *Neuroimage, 57*(1), 113-123.

Dawson, G., Finley, C., Phillips, S., & Galpert, L. (1986). Hemispheric specialization and the language abilities of autistic children. *Child Dev, 57*(6), 1440-1453.

Dawson, G., Finley, C., Phillips, S., & Lewy, A. (1989). A comparison of hemispheric asymmetries in speech-related brain potentials of autistic and dysphasic children. *Brain Lang, 37*(1), 26-41.

De Fosse, L., Hodge, S. M., Makris, N., Kennedy, D. N., Caviness, V. S., Jr., McGrath, L., Steele, S., Ziegler, D. A., Herbert, M. R., Frazier, J. A., Tager-Flusberg, H., & Harris, G. J. (2004). Language-association cortex asymmetry in autism and specific language impairment. *Ann Neurol, 56*(6), 757-766.

de Guibert, C., Maumet, C., Jannin, P., Ferre, J. C., Treguier, C., Barillot, C., Le Rumeur, E., Allaire, C., & Biraben, A. (2011). Abnormal functional lateralization and activity of language brain areas in typical specific language impairment (developmental dysphasia). *Brain, 134*(Pt 10), 3044-3058.

Di Martino, A., Kelly, C., Grzadzinski, R., Zuo, X. N., Mennes, M., Mairena, M. A., Lord, C., Castellanos, F. X., & Milham, M. P. (2011). Aberrant striatal functional connectivity in children with autism. *Biol Psychiatry, 69*(9), 847-856.

Di Martino, A., Yan, C. G., Li, Q., Denio, E., Castellanos, F. X., Alaerts, K., Anderson, J. S., Assaf, M., Bookheimer, S. Y., Dapretto, M., Deen, B., Delmonte, S., Dinstein, I., Ertl-Wagner, B., Fair, D. A., Gallagher, L., Kennedy, D. P., Keown, C. L., Keysers, C., Lainhart, J. E., Lord, C., Luna, B., Menon, V., Minshew, N. J., Monk, C. S., Mueller, S., Muller, R. A., Nebel, M. B., Nigg, J. T., O'Hearn, K., Pelphrey, K. A., Peltier, S. J., Rudie, J. D., Sunaert, S., Thioux, M., Tyszka, J. M., Uddin, L. Q., Verhoeven, J. S., Wenderoth, N., Wiggins, J. L., Mostofsky, S. H., & Milham, M. P. (2013). The autism brain imaging data exchange: Towards a large-scale evaluation of the intrinsic brain architecture in autism. *Mol Psychiatry*, doi:10.1038/mp.2013.1078.

DiMartino, A., Yan, C.-G., Li, Q., Denio, E., Castellanos, F. X., Alaerts, K., Anderson, J. S., Assaf, M., Bookheimer, S. Y., Dapretto, M., Deen, B., Delmonte, S., Dinstein, I., Ertl-Wagner, B., Fair, D. A., Gallagher, L., Kennedy, D. P., Keown, C. L., Keysers, C., Lainhart, J. E., Lord, C., Luna, B., Menon, V., Minshew, N., Monk, C. S., Mueller, S., Müller, R.-A., Nebel, M. B., Nigg, J. T., O'Hearn, K., Pelphrey, K. A., Peltier, S. J., Rudie, J. D., Sunaert, S., Thioux, M., Tyszka, J. M., Uddin, L. Q., Verhoeven, J. S., Wenderoth, N., Wiggins, J. L., Mostofsky, S. H., & Milham, M. P. (2013). The autism brain imaging data exchange: Towards large-scale evaluation of the intrinsic brain architecture in autism. *Molecular Psychiatry, In Press*.

Dinstein, I., Pierce, K., Eyler, L., Solso, S., Malach, R., Behrmann, M., & Courchesne, E. (2011). Disrupted neural synchronization in toddlers with autism. *Neuron, 70*(6), 1218-1225.

Dosenbach, N. U., Fair, D. A., Miezin, F. M., Cohen, A. L., Wenger, K. K., Dosenbach, R. A., Fox, M. D., Snyder, A. Z., Vincent, J. L., Raichle, M. E., Schlaggar, B. L., & Petersen, S. E. (2007). Distinct brain networks for adaptive and stable task control in humans. *Proc Natl Acad Sci U S A, 104*(26), 11073-11078.

Duchesnay, E., Cachia, A., Boddaert, N., Chabane, N., Mangin, J. F., Martinot, J. L., Brunelle, F., & Zilbovicius, M. (2011). Feature selection and classification of imbalanced datasets: Application to pet images of children with autistic spectrum disorders. *NeuroImage, 57*(3), 1003-1014.

Ecker, C., Marquand, A., Mourao-Miranda, J., Johnston, P., Daly, E. M., Brammer, M. J., Maltezos, S., Murphy, C. M., Robertson, D., Williams, S. C., & Murphy, D. G. (2010a). Describing the brain in autism in five dimensions--magnetic resonance imaging-assisted diagnosis of autism spectrum disorder using a multiparameter classification approach. *J Neurosci, 30*(32), 10612-10623.

Ecker, C., Rocha-Rego, V., Johnston, P., Mourao-Miranda, J., Marquand, A., Daly, E. M., Brammer, M. J., Murphy, C., & Murphy, D. G. (2010b). Investigating the predictive value of whole-brain structural mr scans in autism: A pattern classification approach. *Neuroimage, 49*(1), 44-56.

Eyler, L. T., Pierce, K., & Courchesne, E. (2012). A failure of left temporal cortex to specialize for language is an early emerging and fundamental property of autism. *Brain, 135*(Pt 3), 949-960.

Feinberg, D. A., & Yacoub, E. (2012). The rapid development of high speed, resolution and precision in fMRI. *NeuroImage, 62*(2), 720-725.

Ferguson, M. A., & Anderson, J. S. (2011). Dynamical stability of intrinsic connectivity networks. *Neuroimage, 59*(4), 4022-4031.

Ferguson, M. A., & Anderson, J. S. (2012). Dynamical stability of intrinsic connectivity networks. *Neuroimage, 59*(4), 4022-4031.

Ferstl, E. C., Neumann, J., Bogler, C., & von Cramon, D. Y. (2008). The extended language network: A meta-analysis of neuroimaging studies on text comprehension. *Hum Brain Mapp, 29*(5), 581-593.

Fletcher, P. T., Whitaker, R. T., Tao, R., DuBray, M. B., Froehlich, A., Ravichandran, C., Alexander, A. L., Bigler, E. D., Lange, N., & Lainhart, J. E. (2010). Microstructural connectivity of the arcuate fasciculus in adolescents with high-functioning autism. *Neuroimage, 51*(3), 1117-1125.

Fox, M. D., Corbetta, M., Snyder, A. Z., Vincent, J. L., & Raichle, M. E. (2006). Spontaneous neuronal activity distinguishes human dorsal and ventral attention systems. *Proc Natl Acad Sci U S A, 103*(26), 10046-10051.

Fox, M. D., Snyder, A. Z., Vincent, J. L., Corbetta, M., Van Essen, D. C., & Raichle, M. E. (2005). The human brain is intrinsically organized into dynamic, anticorrelated functional networks. *Proc Natl Acad Sci U S A, 102*(27), 9673-9678.

Geranmayeh, F., Brownsett, S. L., Leech, R., Beckmann, C. F., Woodhead, Z., & Wise, R. J. (2012). The contribution of the inferior parietal cortex to spoken language production. *Brain Lang, 121*(1), 47-57.

Gotts, S. J., Jo, H. J., Wallace, G. L., Saad, Z. S., Cox, R. W., & Martin, A. (2013a). Two distinct forms of functional lateralization in the human brain. *Proc Natl Acad Sci U S A*.

Gotts, S. J., Saad, Z. S., Jo, H. J., Wallace, G. L., Cox, R. W., & Martin, A. (2013b). The perils of global signal regression for group comparisons: A case study of autism spectrum disorders. *Front Hum Neurosci, 7*, 356.

Gotts, S. J., Simmons, W. K., Milbury, L. A., Wallace, G. L., Cox, R. W., & Martin, A. (2012). Fractionation of social brain circuits in autism spectrum disorders. *Brain, 135*(Pt 9), 2711-2725.

Greicius, M. D., Boyett-Anderson, J. M., Menon, V., & Reiss, A. L. (2004). Reduced basal forebrain and hippocampal activation during memory encoding in girls with fragile x syndrome. *Neuroreport, 15*(10), 1579-1583.

Gusnard, D. A., Akbudak, E., Shulman, G. L., & Raichle, M. E. (2001). Medial prefrontal cortex and self-referential mental activity: Relation to a default mode of brain function. *Proc Natl Acad Sci U S A, 98*(7), 4259-4264.

Gusnard, D. A., & Raichle, M. E. (2001). Searching for a baseline: Functional imaging and the resting human brain. *Nat Rev Neurosci, 2*(10), 685-694.

Herbert, M. R., Harris, G. J., Adrien, K. T., Ziegler, D. A., Makris, N., Kennedy, D. N., Lange, N. T., Chabris, C. F., Bakardjiev, A., Hodgson, J., Takeoka, M., Tager-Flusberg, H., & Caviness, V. S., Jr. (2002). Abnormal asymmetry in language association cortex in autism. *Ann Neurol, 52*(5), 588-596.

Herbert, M. R., Ziegler, D. A., Deutsch, C. K., O'Brien, L. M., Kennedy, D. N., Filipek, P. A., Bakardjiev, A. I., Hodgson, J., Takeoka, M., Makris, N., & Caviness, V. S., Jr. (2005). Brain asymmetries in autism and developmental language disorder: A nested whole-brain analysis. *Brain, 128*(Pt 1), 213-226.

Herve, P. Y., Zago, L., Petit, L., Mazoyer, B., & Tzourio-Mazoyer, N. (2013). Revisiting human hemispheric specialization with neuroimaging. *Trends Cogn Sci, 17*(2), 69-80.

Ingalhalikar, M., Parker, D., Bloy, L., Roberts, T. P., & Verma, R. (2011). Diffusion based abnormality markers of pathology: Toward learned diagnostic prediction of asd. *NeuroImage, 57*(3), 918-927.

Iturria-Medina, Y., Perez Fernandez, A., Morris, D. M., Canales-Rodriguez, E. J., Haroon, H. A., Garcia Penton, L., Augath, M., Galan Garcia, L., Logothetis, N., Parker, G. J., & Melie-Garcia, L. (2011). Brain hemispheric structural efficiency and interconnectivity rightward asymmetry in human and nonhuman primates. *Cereb Cortex, 21*(1), 56-67.

Iwabuchi, S. J., Haberling, I. S., Badzakova-Trajkov, G., Patston, L. L., Waldie, K. E., Tippett, L. J., Corballis, M. C., & Kirk, I. J. (2011). Regional differences in cerebral asymmetries of human cortical white matter. *Neuropsychologia, 49*(13), 3599-3604.

Jiao, Y., Chen, R., Ke, X., Chu, K., Lu, Z., & Herskovits, E. H. (2010). Predictive models of autism spectrum disorder based on brain regional cortical thickness. *Neuroimage, 50*(2), 589-599.

Jo, H. J., Saad, Z. S., Gotts, S. J., Martin, A., & Cox, R. W. (2013). Correction: Quantifying agreement between anatomical and functional interhemispheric correspondences in the resting brain. *PLoS One, 8*(5).

Just, M. A., Cherkassky, V. L., Keller, T. A., & Minshew, N. J. (2004). Cortical activation and synchronization during sentence comprehension in high-functioning autism: Evidence of underconnectivity. *Brain, 127*(Pt 8), 1811-1821.

Keehn, B., Shih, P., Brenner, L. A., Townsend, J., & Muller, R. A. (2012). Functional connectivity for an "island of sparing" in autism spectrum disorder: An fMRI study of visual search. *Hum Brain Mapp,* doi: 10.1002/hbm.22084.

Kennedy, D. P., & Courchesne, E. (2008a). Functional abnormalities of the default network during self- and other-reflection in autism. *Soc Cogn Affect Neurosci, 3*(2), 177-190.

Kennedy, D. P., & Courchesne, E. (2008b). The intrinsic functional organization of the brain is altered in autism. *Neuroimage, 39*(4), 1877-1885.

Kennedy, D. P., Redcay, E., & Courchesne, E. (2006). Failing to deactivate: Resting functional abnormalities in autism. *Proc Natl Acad Sci U S A, 103*(21), 8275-8280.

Khan, S., Gramfort, A., Shetty, N. R., Kitzbichler, M. G., Ganesan, S., Moran, J. M., Lee, S. M., Gabrieli, J. D., Tager-Flusberg, H. B., Joseph, R. M., Herbert, M. R., Hamalainen, M. S., & Kenet, T. (2013). Local and long-range functional connectivity is reduced in concert in autism spectrum disorders. *Proc Natl Acad Sci U S A, 110*(8), 3107-3112.

Kleinhans, N. M., Muller, R. A., Cohen, D. N., & Courchesne, E. (2008a). Atypical functional lateralization of language in autism spectrum disorders. *Brain Research, 1221*, 115-125.

Kleinhans, N. M., Muller, R. A., Cohen, D. N., & Courchesne, E. (2008). Atypical functional lateralization of language in autism spectrum disorders. *Brain Res, 1221*, 115-125.

Kleinhans, N. M., Richards, T., Sterling, L., Stegbauer, K. C., Mahurin, R., Johnson, L. C., Greenson, J., Dawson, G., & Aylward, E. (2008). Abnormal functional connectivity in autism spectrum disorders during face processing. *Brain, 131*(Pt 4), 1000-1012.

Knaus, T. A., Silver, A. M., Kennedy, M., Lindgren, K. A., Dominick, K. C., Siegel, J., & Tager-Flusberg, H. (2010). Language laterality in autism spectrum disorder and typical controls: A functional, volumetric, and diffusion tensor MRI study. *Brain Lang, 112*(2), 113-120.

Knaus, T. A., Silver, A. M., Lindgren, K. A., Hadjikhani, N., & Tager-Flusberg, H. (2008). fMRI activation during a language task in adolescents with asd. *J Int Neuropsychol Soc, 14*(6), 967-979.

Knecht, S., Deppe, M., Drager, B., Bobe, L., Lohmann, H., Ringelstein, E., & Henningsen, H. (2000a). Language lateralization in healthy right-handers. *Brain, 123 (Pt 1)*, 74-81.

Knecht, S., Drager, B., Deppe, M., Bobe, L., Lohmann, H., Floel, A., Ringelstein, E. B., & Henningsen, H. (2000b). Handedness and hemispheric language dominance in healthy humans. *Brain, 123 Pt 12*, 2512-2518.

Koshino, H., Carpenter, P. A., Minshew, N. J., Cherkassky, V. L., Keller, T. A., & Just, M. A. (2005). Functional connectivity in an fmri working memory task in high-functioning autism. *Neuroimage, 24*(3), 810-821.

Kovalev, V. A., Kruggel, F., & von Cramon, D. Y. (2003). Gender and age effects in structural brain asymmetry as measured by mri texture analysis. *Neuroimage, 19*(3), 895-905.

Kraemer, H. C., Yesavage, J. A., Taylor, J. L., & Kupfer, D. (2000). How can we learn about developmental processes from cross-sectional studies, or can we? *Am J Psychiatry, 157*(2), 163-171.

Kucyi, A., Hodaie, M., & Davis, K. D. (2012). Lateralization in intrinsic functional connectivity of the temporoparietal junction with salience- and attention-related brain networks. *J Neurophysiol, 108*(12), 3382-3392.

Lange, N., DuBray, M., Lee, J. E., Froimowitz, M., Froehlich, A., Adluru, N., Wright, B., Ravichandran, C., Fletcher, T., Bigler, E., Alexander, A., & Lainhart, J. (2010a). Atypical diffusion tensor hemispheric asymmetry: A potential dti biomarker for autism. *Autism Research, 3*(6), 350-358.

Lange, N., Dubray, M. B., Lee, J. E., Froimowitz, M. P., Froehlich, A., Adluru, N., Wright, B., Ravichandran, C., Fletcher, P. T., Bigler, E. D., Alexander, A. L., & Lainhart, J. E. (2010b). Atypical diffusion tensor hemispheric asymmetry in autism. *Autism Res, 3*(6), 350-358.

Lee, J. E., Bigler, E. D., Alexander, A. L., Lazar, M., DuBray, M. B., Chung, M. K., Johnson, M., Morgan, J., Miller, J. N., McMahon, W. M., Lu, J., Jeong, E. K., & Lainhart, J. E. (2007). Diffusion tensor imaging of white matter in the superior temporal gyrus and temporal stem in autism. *Neuroscience Letters, 424*(2), 127-132.

LeMay, M. (1977). Asymmetries of the skull and handedness. Phrenology revisited. *J Neurol Sci, 32*(2), 243-253.

Liu, H., Stufflebeam, S. M., Sepulcre, J., Hedden, T., & Buckner, R. L. (2009). Evidence from intrinsic activity that asymmetry of the human brain is controlled by multiple factors. *Proc Natl Acad Sci U S A, 106*(48), 20499-20503.

Lo, Y. C., Soong, W. T., Gau, S. S., Wu, Y. Y., Lai, M. C., Yeh, F. C., Chiang, W. Y., Kuo, L. W., Jaw, F. S., & Tseng, W. Y. (2011). The loss of asymmetry and reduced interhemispheric connectivity in adolescents with autism: A study using diffusion spectrum imaging tractography. *Psychiatry Res, 192*(1), 60-66.

Lord, C., Risi, S., Lambrecht, L., Cook, E. H., Jr., Leventhal, B. L., DiLavore, P. C., Pickles, A., & Rutter, M. (2000). The autism diagnostic observation schedule-generic: A standard measure of social and communication deficits associated with the spectrum of autism. *J Autism Dev Disord, 30*(3), 205-223.

Lord, C., Rutter, M., & Le Couteur, A. (1994). Autism diagnostic interview-revised: A revised version of a diagnostic interview for caregivers of individuals with possible pervasive developmental disorders. *J Autism Dev Disord, 24*(5), 659-685.

Lynch, C. J., Uddin, L. Q., Supekar, K., Khouzam, A., Phillips, J., & Menon, V. (2013). Default mode network in childhood autism: Posteromedial cortex heterogeneity and relationship with social deficits. *Biol Psychiatry, 74*(3), 212-219.

Margulies, D. S., Vincent, J. L., Kelly, C., Lohmann, G., Uddin, L. Q., Biswal, B. B., Villringer, A., Castellanos, F. X., Milham, M. P., & Petrides, M. (2009). Precuneus shares intrinsic functional architecture in humans and monkeys. *Proc Natl Acad Sci U S A, 106*(47), 20069-20074.

Mayer, J. S., Roebroeck, A., Maurer, K., & Linden, D. E. (2010). Specialization in the default mode: Task-induced brain deactivations dissociate between visual working memory and attention. *Hum Brain Mapp, 31*(1), 126-139.

Monk, C. S., Peltier, S. J., Wiggins, J. L., Weng, S. J., Carrasco, M., Risi, S., & Lord, C. (2009). Abnormalities of intrinsic functional connectivity in autism spectrum disorders. *Neuroimage, 47*(2), 764-772.

Mostofsky, S. H., Powell, S. K., Simmonds, D. J., Goldberg, M. C., Caffo, B., & Pekar, J. J. (2009a). Decreased connectivity and cerebellar activity in autism during motor task performance. *Brain, 132*, 2413-2425.

Mostofsky, S. H., Powell, S. K., Simmonds, D. J., Goldberg, M. C., Caffo, B., & Pekar, J. J. (2009b). Decreased connectivity and cerebellar activity in autism during motor task performance. *Brain, 132*(Pt 9), 2413-2425.

Muller, R. A., Behen, M. E., Rothermel, R. D., Chugani, D. C., Muzik, O., Mangner, T. J., & Chugani, H. T. (1999). Brain mapping of language and auditory perception in high-functioning autistic adults: A pet study. *J Autism Dev Disord, 29*(1), 19-31.

Muller, R. A., Shih, P., Keehn, B., Deyoe, J. R., Leyden, K. M., & Shukla, D. K. (2011). Underconnected, but how? A survey of functional connectivity mri studies in autism spectrum disorders. *Cereb Cortex, 21*(10), 2233-2243.

Murphy, K., Birn, R. M., Handwerker, D. A., Jones, T. B., & Bandettini, P. A. (2009). The impact of global signal regression on resting state correlations: Are anti-correlated networks introduced? *Neuroimage, 44*(3), 893-905.

Nielsen, J. A., Zielinski, B. A., Ferguson, M. A., Lainhart, J. E., & Anderson, J. S. (2013). An evaluation of the left-brain vs. Right-brain hypothesis with resting state functional connectivity magnetic resonance imaging. *PLoS One, 8*(8), e71275.

Northoff, G., Heinzel, A., de Greck, M., Bermpohl, F., Dobrowolny, H., & Panksepp, J. (2006). Self-referential processing in our brain--a meta-analysis of imaging studies on the self. *Neuroimage, 31*(1), 440-457.

Oertel-Knochel, V., & Linden, D. E. (2011). Cerebral asymmetry in schizophrenia. *Neuroscientist, 17*(5), 456-467.

Power, J. D., Barnes, K. A., Snyder, A. Z., Schlaggar, B. L., & Petersen, S. E. (2012). Spurious but systematic correlations in functional connectivity mri networks arise from subject motion. *Neuroimage, 59*(3), 2142-2154.

Raichle, M. E., MacLeod, A. M., Snyder, A. Z., Powers, W. J., Gusnard, D. A., & Shulman, G. L. (2001). A default mode of brain function. *Proc Natl Acad Sci U S A, 98*(2), 676-682.

Redcay, E., & Courchesne, E. (2008). Deviant functional magnetic resonance imaging patterns of brain activity to speech in 2-3-year-old children with autism spectrum disorder. *Biol Psychiatry, 64*(7), 589-598.

Roberts, T. P., Cannon, K. M., Tavabi, K., Blaskey, L., Khan, S. Y., Monroe, J. F., Qasmieh, S., Levy, S. E., & Edgar, J. C. (2011). Auditory magnetic mismatch field latency: A biomarker for language impairment in autism. *Biol Psychiatry, 70*(3), 263-269.

Roberts, T. P., Khan, S. Y., Rey, M., Monroe, J. F., Cannon, K., Blaskey, L., Woldoff, S., Qasmieh, S., Gandal, M., Schmidt, G. L., Zarnow, D. M., Levy, S. E., & Edgar, J. C. (2010). Meg detection of delayed auditory evoked responses in autism spectrum disorders: Towards an imaging biomarker for autism. *Autism Res, 3*(1), 8-18.

Saad, Z., Reynolds, R. C., Jo, H. J., Gotts, S. J., Chen, G., Martin, A., & Cox, R. (2013). Correcting brain-wide correlation differences in resting-state fMRI. *Brain Connect, In Press*.

Saad, Z. S., Gotts, S. J., Murphy, K., Chen, G., Jo, H. J., Martin, A., & Cox, R. W. (2012). Trouble at rest: How correlation patterns and group differences become distorted after global signal regression. *Brain Connect, 2*(1), 25-32.

Saenger, V. M., Barrios, F. A., Martinez-Gudino, M. L., & Alcauter, S. (2012). Hemispheric asymmetries of functional connectivity and grey matter volume in the default mode network. *Neuropsychologia, 50*(7), 1308-1315.

Sato, J. R., Hoexter, M. Q., Oliveira, P. P., Jr., Brammer, M. J., Murphy, D., & Ecker, C. (2013). Inter-regional cortical thickness correlations are associated with autistic symptoms: A machine-learning approach. *J Psychiatr Res, 47*(4), 453-459.

Satterthwaite, T. D., Elliott, M. A., Gerraty, R. T., Ruparel, K., Loughead, J., Calkins, M. E., Eickhoff, S. B., Hakonarson, H., Gur, R. C., Gur, R. E., & Wolf, D. H. (2013). An improved framework for confound regression and filtering for control of motion artifact in the preprocessing of resting-state functional connectivity data. *Neuroimage, 64*, 240-256.

Saxe, R., & Kanwisher, N. (2003). People thinking about thinking people. The role of the temporo-parietal junction in "theory of mind." *Neuroimage, 19*(4), 1835-1842.

Seeley, W. W., Menon, V., Schatzberg, A. F., Keller, J., Glover, G. H., Kenna, H., Reiss, A. L., & Greicius, M. D. (2007). Dissociable intrinsic connectivity networks for salience processing and executive control. *J Neurosci, 27*(9), 2349-2356.

Seery, A. M., Vogel-Farley, V., Tager-Flusberg, H., & Nelson, C. A. (2013). Atypical lateralization of erp response to native and non-native speech in infants at risk for autism spectrum disorder. *Developmental Cognitive Neuroscience, 5*, 10-24.

Seghier, M. L. (2008). Laterality index in functional MRI: Methodological issues. *Magn Reson Imaging, 26*(5), 594-601.

Seghier, M. L., Fagan, E., & Price, C. J. (2010). Functional subdivisions in the left angular gyrus where the semantic system meets and diverges from the default network. *J Neurosci, 30*(50), 16809-16817.

Sestieri, C., Corbetta, M., Romani, G. L., & Shulman, G. L. (2011). Episodic memory retrieval, parietal cortex, and the default mode network: Functional and topographic analyses. *J Neurosci, 31*(12), 4407-4420.

Setsompop, K., Gagoski, B. A., Polimeni, J. R., Witzel, T., Wedeen, V. J., & Wald, L. L. (2012). Blipped-controlled aliasing in parallel imaging for simultaneous multislice echo planar imaging with reduced g-factor penalty. *Magn Reson Med, 67*(5), 1210-1224.

Shehzad, Z., Kelly, A. M., Reiss, P. T., Gee, D. G., Gotimer, K., Uddin, L. Q., Lee, S. H., Margulies, D. S., Roy, A. K., Biswal, B. B., Petkova, E., Castellanos, F. X., &

Milham, M. P. (2009). The resting brain: Unconstrained yet reliable. *Cereb Cortex, 19*(10), 2209-2229.

Shulman, G. L., Pope, D. L., Astafiev, S. V., McAvoy, M. P., Snyder, A. Z., & Corbetta, M. (2010). Right hemisphere dominance during spatial selective attention and target detection occurs outside the dorsal frontoparietal network. *J Neurosci, 30*(10), 3640-3651.

Sparrow, S. S., Balla, D. A., & Cicchetti, D. (1984). *Vineland adaptive behavior scales*. Circle Pines, M.N.: American Guidance Service.

Sporns, O., Honey, C. J., & Kotter, R. (2007). Identification and classification of hubs in brain networks. *PLoS One, 2*(10), e1049.

Stephan, K. E., Marshall, J. C., Friston, K. J., Rowe, J. B., Ritzl, A., Zilles, K., & Fink, G. R. (2003). Lateralized cognitive processes and lateralized task control in the human brain. *Science, 301*(5631), 384-386.

Szaflarski, J. P., Binder, J. R., Possing, E. T., McKiernan, K. A., Ward, B. D., & Hammeke, T. A. (2002). Language lateralization in left-handed and ambidextrous people: fMRI data. *Neurology, 59*(2), 238-244.

Tesink, C. M., Buitelaar, J. K., Petersson, K. M., van der Gaag, R. J., Kan, C. C., Tendolkar, I., & Hagoort, P. (2009a). Neural correlates of pragmatic language comprehension in autism spectrum disorders. *Brain, 132*(Pt 7), 1941-1952.

Tesink, C. M., Petersson, K. M., van Berkum, J. J., van den Brink, D., Buitelaar, J. K., & Hagoort, P. (2009b). Unification of speaker and meaning in language comprehension: An fMRI study. *J Cogn Neurosci, 21*(11), 2085-2099.

Tian, L., Wang, J., Yan, C., & He, Y. (2011). Hemisphere- and gender-related differences in small-world brain networks: A resting-state functional mri study. *Neuroimage, 54*(1), 191-202.

Toga, A. W., & Thompson, P. M. (2003). Mapping brain asymmetry. *Nat Rev Neurosci, 4*(1), 37-48.

Tomasi, D., & Volkow, N. D. (2012a). Language network: Segregation, laterality and connectivity. *Mol Psychiatry, 17*(8), 759.

Tomasi, D., & Volkow, N. D. (2012b). Laterality patterns of brain functional connectivity: Gender effects. *Cereb Cortex, 22*(6), 1455-1462.

Travers, B. G., Adluru, N., Ennis, C., Tromp do, P. M., Destiche, D., Doran, S., Bigler, E. D., Lange, N., Lainhart, J. E., & Alexander, A. L. (2012). Diffusion tensor imaging in autism spectrum disorder: A review. *Autism Res, 5*(5), 289-313.

Tsiaras, V., Simos, P. G., Rezaie, R., Sheth, B. R., Garyfallidis, E., Castillo, E. M., & Papanicolaou, A. C. (2011). Extracting biomarkers of autism from meg resting-state functional connectivity networks. *Comput Biol Med, 41*(12), 1166-1177.

Tyszka, J. M., Kennedy, D. P., Paul, L. K., & Adolphs, R. (2013). Largely typical patterns of resting-state functional connectivity in high-functioning adults with autism. *Cereb Cortex*, doi: 10.1093/cercor/bht1040.

Uddin, L. Q., Menon, V., Young, C. B., Ryali, S., Chen, T., Khouzam, A., Minshew, N. J., & Hardan, A. Y. (2011). Multivariate searchlight classification of structural magnetic resonance imaging in children and adolescents with autism. *Biol Psychiatry, 70*(9), 833-841.

Van Dijk, K. R., Hedden, T., Venkataraman, A., Evans, K. C., Lazar, S. W., & Buckner, R. L. (2010). Intrinsic functional connectivity as a tool for human connectomics: Theory, properties, and optimization. *J Neurophysiol, 103*(1), 297-321.

Van Dijk, K. R., Sabuncu, M. R., & Buckner, R. L. (2012). The influence of head motion on intrinsic functional connectivity mri. *Neuroimage, 59*(1), 431-438.

Villalobos, M. E., Mizuno, A., Dahl, B. C., Kemmotsu, N., & Muller, R. A. (2005). Reduced functional connectivity between v1 and inferior frontal cortex associated with visuomotor performance in autism. *Neuroimage, 25*(3), 916-925.

von dem Hagen, E. A., Stoyanova, R. S., Baron-Cohen, S., & Calder, A. J. (2012). Reduced functional connectivity within and between 'social' resting state networks in autism spectrum conditions. *Soc Cogn Affect Neurosci,* doi:10.1093/scan/nss053.

Wang, H., Chen, C., & Fushing, H. (2012). Extracting multiscale pattern information of fMRI based functional brain connectivity with application on classification of autism spectrum disorders. *PLoS One, 7*(10), e45502.

Watkins, K. E., Paus, T., Lerch, J. P., Zijdenbos, A., Collins, D. L., Neelin, P., Taylor, J., Worsley, K. J., & Evans, A. C. (2001). Structural asymmetries in the human brain: A voxel-based statistical analysis of 142 MRI scans. *Cereb Cortex, 11*(9), 868-877.

Welchew, D. E., Ashwin, C., Berkouk, K., Salvador, R., Suckling, J., Baron-Cohen, S., & Bullmore, E. (2005). Functional disconnectivity of the medial temporal lobe in asperger's syndrome. *Biol Psychiatry, 57*(9), 991-998.

Weng, S. J., Wiggins, J. L., Peltier, S. J., Carrasco, M., Risi, S., Lord, C., & Monk, C. S. (2010). Alterations of resting state functional connectivity in the default network in adolescents with autism spectrum disorders. *Brain Res, 1313*, 202-214.

Wiggins, J. L., Peltier, S. J., Ashinoff, S., Weng, S. J., Carrasco, M., Welsh, R. C., Lord, C., & Monk, C. S. (2011). Using a self-organizing map algorithm to detect age-related changes in functional connectivity during rest in autism spectrum disorders. *Brain Res, 1380*, 187-197.

Yeo, B. T., Krienen, F. M., Sepulcre, J., Sabuncu, M. R., Lashkari, D., Hollinshead, M., Roffman, J. L., Smoller, J. W., Zollei, L., Polimeni, J. R., Fischl, B., Liu, H., & Buckner, R. L. (2011). The organization of the human cerebral cortex estimated by intrinsic functional connectivity. *J Neurophysiol, 106*(3), 1125-1165.

Zielinski, B. A., Anderson, J. S., Froehlich, A. L., Prigge, M. B., Nielsen, J. A., Cooperrider, J. R., Cariello, A. N., Fletcher, P. T., Alexander, A. L., & Lange, N. (2012). scMRI reveals large-scale brain network abnormalities in autism. *PLoS One, 7*(11), e49172.

Zielinski, B. A., Gennatas, E. D., Zhou, J., & Seeley, W. W. (2010). Network-level structural covariance in the developing brain. *Proc Natl Acad Sci U S A, 107*(42), 18191-18196.